UNIVERSITY COLLEGE OF SOUTHEAST NORWAY

Master Thesis

Dual frequency ultrasound transducer array

BIKASH KUMAR CHAUDHARY

Supervisor: Prof. Lars Hoff

Co- Supervisor: Dr.Tung Manh, Kenneth Andersen, Rumin Chen

Faculty of Technology and Maritime Science University College of Southeast Norway

January 2017

ABSTRACT

Ultrasound imaging has become one of the most widely used diagnostic tools because it is safe, less expensive, produce real time image. Ultrasound technology has been widely used for a broad range of applications including medical imaging. An ultrasound transducer is one of the most important components in a medical ultrasound imaging system. This device interacts with the human body by creating the sound waves and receiving the echoes. An ultrasonic array transducer is a single transducer that contains a number of individually connected elements. Recent years have seen a dramatic improvement in the use of ultrasonic array transducers for medical applications. Variations of the individual elements from their ideal state will have significant effects on the performance of the linear array transducers.

The aim is to design, fabricate and test a prototype dual frequency ultrasound array. The array shall be based on an acoustic stack with two piezoelectric layers, one 'pumping' low frequency at around 4 MHz, and one 'imaging' high frequency, around 20 MHz. This thesis studies the design and characteristic of both the transducer array. Piezoelectric material i.e. (Pzt-27) has been used as an active layer for 4 Mhz transducer and Fuji c-82 has been used as an active layer for 20 Mhz transducer. Performance parameters of importance in transducer design are considered, including sensitivity, coupling constant, band width, frequency downshift beam and electrical matching. Impedance measurement for the both transducer has been measured and compared.

ACKNOWLEDGMENT

First of all I would like to thank my supervisors, Professor Lars Hoff for guiding me through the work with my Thesis. Professor Lars support has been invaluable to my work. His knowledge, energy, optimism, patience and belief in me have been of great importance to me and for my work. He is always available for discussion, and has always respected my opinion and listened to me. I am very grateful to have had the opportunity to work with him.

The support of Dr.Tung Manh has been of great importance in completing this work. He has made sure that I at any time have kept my focus on working towards the goal of finishing my thesis on time.

Researcher Kenneth Andersen is besides Professor lars, the person who I have worked the closest with during my thesis. His interest in my work and positive spirit has been very important to me, especially in times of frustration and despair. I would also like to thank Dr. Rumin chen for the support in the lab and for fruitful discussion. He is an incredible source of knowledge and is always available for discussion and explaining the mysteries of ultrasound.

It has been a great experience to get to work with the group of Professor Lars Hoff, and I would like to thank the rest of the group. It has been a pleasure working with such great individuals, with their knowledge and interest for medical ultrasound. Last but not least, I am grateful beyond words to my friends and my family. Their jokes, encouragement and continuous support helped me stay optimistic and happy during this master study.

Bikash Kumar Chaudhary

Contents

List of Figures

List of Table

1 CHAPTER INTRODUCTION

1.1 ULTRASOUND IN MEDICAL IMAGING

The potential of ultrasound as an imaging modality was realized as early as the late 1940s when, utilizing sonar and radar technology developed during World War II, several groups of investigators around the world started exploring diagnostic capabilities of ultrasound [12]. Ultrasonic devices are used to detect/image objects and measure distances. In nondestructive testing (NDT) method, ultrasound is used to detect invisible flaws and measure thickness of objects without harming the objects [13]. In the early 1950s, John Wild and John Reid in Minnesota developed a prototype B-mode ultrasonic imaging instrument and were able to demonstrate the capability of ultrasound for imaging and characterization of cancerous tissues at frequencies as high as 15 MHz [12]. The primary form of ultrasonic imaging to date has been that of a pulse–echo mode. The principle is very similar to that of sonar and radar. In essence, following an ultrasonic pulse transmission, echoes from the medium being interrogated are detected and used to form an image. Much of the terminology used in ultrasound was imported from the field of sonar and radar. Ultrasound was discovered as a potential imaging ability since the 1940s [14]. Then, ultrasound has been applied for numerous medical applications. It was accepted as a powerful diagnostic tool during the 1970s. Since then, ultrasounds are applied in all the fields of the medicine (the diagnostics in the field of Radiology, cardiology, ophthalmology and orthopedics) [15].

Fundamentally, ultrasound images are visual representations of the interaction between sound waves and the medium of wave propagation. In ultrasound imaging, an acoustic pulse is transmitted into the medium using a transducer capable of producing a temporally short mechanical wave (1–4 cycles) in response to a voltage applied to the transducer. As the incident wave travels into tissue, some of the wave's energy is reflected back toward the transducer by scatterers in the tissue having different acoustic properties (i.e., density and speed of sound) than the background medium. These backscattered acoustic waves are received by the same transducer, which converts mechanical waves into time-varying voltages. These signals are then amplified, digitized, and processed into an image by the ultrasound imaging system. In the most

common mode of operation, called “brightness-mode” or “B-mode” ultrasound, grayscale images are formed in which pixel values are proportional to the brightness of scattered acoustic waves. Ultrasound not only complements the more traditional approaches such as x-ray, but also possesses unique characteristics that are advantageous in comparison to other competing modalities such as x-ray computed tomography (CT), radionuclide emission tomography, and magnetic resonance imaging (MRI). More specifically:

- Ultrasound is a form of nonionizing radiation and is considered safe to the best of present knowledge.
- It is less expensive than imaging modalities of similar capabilities.
- It produces images in real time, unattainable at the present time by any other methods.
- It has a resolution in the millimeter range for the frequencies being clinically used today, which may be improved if the frequency is increased.
- It can yield blood flow information by applying the Doppler principle.
- It is portable and thus can be easily transported to the bedside of a patient.

Ultrasound also has several drawbacks. Chief among them are:

- Organs containing gases and bony structures cannot be adequately imaged without introducing specialized procedures.
- Only a limited window is available for ultrasonic examination of certain organs, such as heart and brain.
- It depends on operator skill.
- It is sometimes impossible to obtain good images from certain types of patients, including obese patients.

The study of this thesis mainly focused on fabrication and test of a prototype dual frequency ultrasound array. The array shall be based on an acoustic stack with two piezoelectric layers, one ‘pumping’ low frequency at around 4 MHz, and one ‘imaging’ high frequency, around 20 MHz. The transducer is made for nonlinear applications, using the high frequency for imaging and the low frequency to manipulate the tissue or for combined imaging and therapy. Applications for this transducer are SURF imaging, combined imaging and drug delivery using bubbles, and monitoring of bubble clouds. The imaging frequency shall be optimized for image resolution, i.e.

high bandwidth and short pulses. The pumping frequency shall be optimized for transmit efficiency, and a high bandwidth is not needed. The proposed structure is a low frequency PZT plate with light backing for sensitivity, with some extra acoustic matching if found beneficial. The high frequency imaging array will be on top of the low frequency stack, with a soft isolation layer of e.g. RTV to block the high frequency part from the low frequency stack.

1.2 Objective of this thesis

Design and modeling

- Design and model ultrasound transducer in a Mason equivalent circuit model, using the available Xtrans software package written in Matlab .
- Simulate the structure in FEM, using COMSOL.
- Model the beam pattern in Field II.

Fabrication

- Evaluate fabrication opportunities, availability of tools and materials.
- Fabricate the low frequency part.
- Fabricate the high frequency.

Array Characterization

- Test the low and high frequency parts separately, using electrical impedance and pulse-echo measurements.
- Join low and high frequency parts, and test the combined structure.
- Find sensitivity, pulse shapes and bandwidth from pulse-echo measurements.

1.3 Outline of this thesis

This thesis is organized as follows Chapter 1 presents an introduction including the background and motivation, the review of previous work, and the thesis objectives. Chapter 2 presents the theoretical background as well as the literature review of the previously proposed studies in relation to ultrasound transducers. Chapter 3 describes the fabrication method of both high and low frequency transducer array and also the FEM simulation using comsol multiphysics and also beam forming using Field II. Chapter 4 is all about measured result and comparing them with simulated result. Chapter 5 contains discussion, outlining challenges and sources of error. Finally, the conclusion of this thesis and the suggestion for future work are presented in Chapter 6.

2 CHAPTER THEORETICAL BACKGROUND

2.1 Acoustic wave propagation

2.1.1 Longitudinal wave and transverse wave

There are two basic types of acoustic waves: longitudinal wave and transverse wave. In longitudinal wave (e.g. the P-wave of the earthquake), the displacement of the medium is parallel to the propagation direction of the wave. In transverse wave S-waves exist in solids only, p-waves in all media, the displacement of the medium is perpendicular to the direction of wave propagation. The speed of mechanical waves propagated through a medium (solid, liquid, or gas) depends on the properties of that medium.

In homogeneous solid medium, the speed of longitudinal wave and the transverse wave can be calculated as follow.

$$V_p = \sqrt{\frac{M}{\rho}} \ , \ V_s = \sqrt{\frac{G}{\rho}} \tag{2.1}$$

where V_p is the speed of longitudinal wave and V_s is the speed of transverse wave in the solid medium. M, G, ρ are P-wave modulus, Shear modulus and density of the medium, respectively. P-wave modulus is defined as the ratio of axial stress to axial strain in a uniaxial strain state. Shear modulus, denoted by G, is defined as the ratio of shear stress to the shear strain, and can be calculated as

$$G = F / A = \frac{Fl}{\Delta x / l \quad A\Delta x} \tag{2.2}$$

transverse direction and L is the initial length. (Figure 2.1)

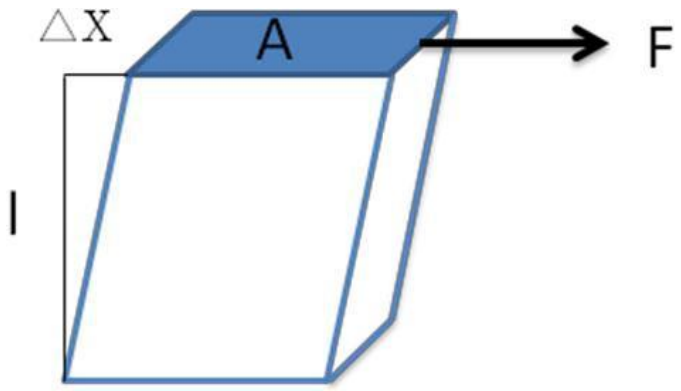

Figure 2.1:The sketch of shear strain and shear stress causing a transverse s-wave..

.

In liquid or gas, the shear modulus is small enough to be recognized as zero. That is because when a force, F, was applied on the fluid or gas, the ∆x will be infinite large and makes the G close to zero. As a result, in liquid or gas, there is only longitudinal wave. The speed of longitudinal wave can be calculated as follow.

$$c = Vp = \sqrt{\frac{M}{\rho}} = \sqrt{\frac{K + {}^{4}/_{3}G}{\rho}} = \sqrt{\frac{K}{\rho}} \quad (2.3)$$

Where c is the speed of wave, V_p is the speed of longitudinal wave, K is the Bulk modulus of the medium. Last term in the right side of the equation is valid for G<<K.

2.2 PIEZOELECTRIC EFFECT

The piezoelectric (pressure-electric) effect is a phenomenon in which a material, upon the application of an electrical field, changes its physical dimensions and vice versa. The piezoelectric effect was discovered by French physicists Pierre and Jacques Curie in 1880. The direct and reverse piezoelectric effects are illustrated in Figure 2.2(a) and (b), respectively. The direct effect refers to the phenomenon in which the application of a stress causes a net charge to

appear across the electrodes and the inverse effect concerns the production of a strain upon the application of a potential difference across the electrodes. Certain naturally occurring crystals such as quartz and tourmaline are piezoelectric.

The physical reason that the piezoelectric phenomenon occurs can be idealistically explained by considering that a piezoelectric material consists of innumerable electric dipoles. When undisturbed, these dipoles are randomly distributed, resulting in a neutral state or no net charge. An electrical potential difference applied across a slab of piezoelectric material realigns the dipoles in the material in a preferential direction and results in a deformation or a change in the thickness of the slab. Conversely, a stress that causes a deformation of the material and reorientation of the dipoles induces a net charge across the electrodes.

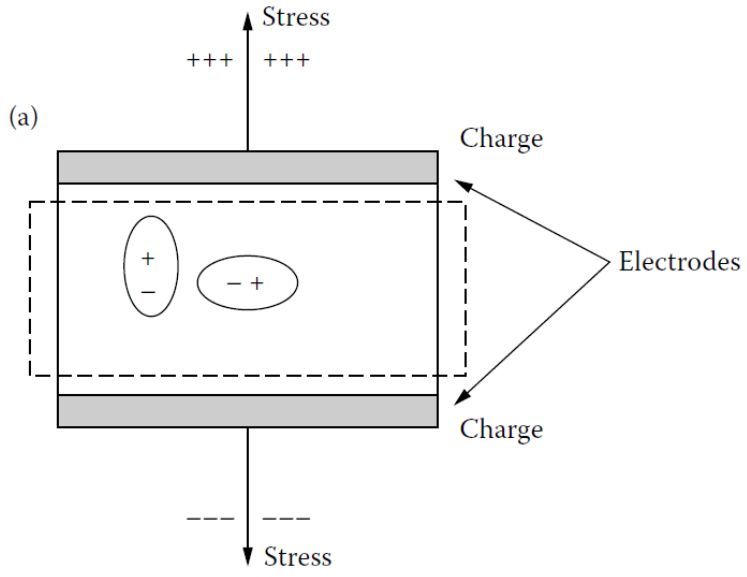

Direct Piezoelectric Effect

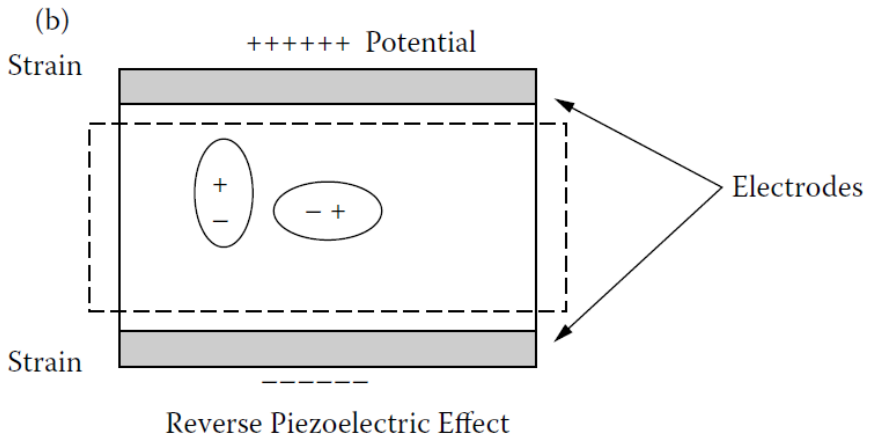

Figure 2.2: (a) Direct piezoelectric effect in which a stress induces a charge separation (b) Reverse piezoelectric effect in which a potential difference across the electrodes induces a strain.

2.3 Principles of the ultrasonic transducer

Almost all ultrasonic transducers today use piezoelectric active elements, and operate based on both converse and direct effects of piezoelectric materials in which the vibration would be produced upon the application of a potential difference across the electrodes and then the signal would be generated when receiving an echo. Consequently, piezoelectric elements play a very important role in transducer technology. For specific applications, proper piezoelectric materials are chosen according to a number of factors such as their piezoelectric performance, dielectric properties, elastic properties and stability

A transducer rings at its natural frequency once it is excited by an electrical source. Since the piezoelectric material itself exhibits much higher characteristic acoustic impedance (~30 MRayl) than that of biological tissue or water (~1.5 MRayl), a substantial part of the acoustic energy would be reflected at the front interface and not propagated into the load material, resulting in poor resolution and sensitivity, if not properly matched acoustically. Loss towards the rear depends on backing. A lossy backing material can be used to increases bandwidth at the cost of low sensitivity Poor matching increases ringing, and reduces energy transfer and bandwidth. Air backing increases the sensitivity and reduces the bandwidth; Heavy (lossy) backing reduces sensitivity. Therefore, the performance of a transducer can be tuned and improved by adding

layers to the front and back of an active layer. The first one is known as matching layer in the front for improving the energy transmission between the active layer and load medium. Backing layer supports the active element and can minimizes ultrasound energy reflected from the backing layer, thus damping out the reverberations, but also reducing sensitivity. The criteria of these mechanical layers are presented in the next section. A typical piezoelectric transducer is shown in figure 2.3.

Figure 2.3: A schematic of a typical piezoelectric transducer

2.4 MECHANICAL MATCHING

When a transducer is excited by an electrical source, it rings at its natural resonant frequency. For continuous-wave application, the transducers are air backed, allowing as much energy irradiated into the forward direction as possible. Due to the mismatch in acoustic impedance between the air and the piezoelectric material, acoustic energy at this interface is reflected into the forward direction. Thus, very little energy is lost out of the back port. The drawback is that this mismatch, which produces the so-called ringing effect for pulse–echo applications, is very undesirable because it lengthens the pulse duration.

Absorptive backing materials with acoustic impedance similar to that of the piezoelectric material can be used to damp out the ringing or to increase bandwidth. The backing material should not only absorb part of the energy from the vibration of the back face but also minimize the mismatch in acoustic impedance. It absorbs as much as possible of the energy that enters it. It must be noted that suppression of ringing or shortening of pulse duration is achieved by sacrificing sensitivity because a large portion of the energy is absorbed by the backing material

The performance of a transducer can also be improved by using acoustic matching layers in the front. It can be shown that, for a monochromatic plane wave, 100% transmission occurs for a layer of material of λm/4 thickness and acoustic impedance Zm, where λm is the wavelength in the matching layer material[5],[6].

$$Z_m = (Z_p Z_l)^{1/2} \tag{2.4}$$

For wideband transducers, Desilets, et al. [6] showed that the optimum impedance of single matching layer should be modified to:

$$Z_m = (Z_p {Z_l}^2)^{1/3} \tag{2.5}$$

And for transducers with two matching layers, the acoustic impedances of these two layers should be:

$$Z_m = ({Z_p}^4 {Z_l}^3)^{1/7} \tag{2.6}$$

$$Z_m = (Z_p {Z_l}^6)^{1/7} \tag{2.7}$$

Similarly, the pressure wave moves backward and reaches the rear surface of piezoelectric element at a normal incidence. A fraction of energy will be transmitted into the air and the rest is reflected back. The reflection coefficient is calculated as follows:

$$R = \frac{Z_a - Z_p}{Z_a + Z_p} \tag{2.8}$$

Where Z_a is the acoustic impedance of air. Large amount of energy will be reflected and reverberate inside the piezoelectric element, creating a long ring down (narrow bandwidth). Therefore, backing layer is used to damp out the ringing due to acoustic impedance mismatch between the air and piezoelectric materials. Theoretically, when the acoustic impedance of the backing Z_b is equal to that of piezoelectric element Z_p, R = 0, a large part of the energy will be lost in the backing, and the sensitivity will be significantly decreased. Therefore, a trade-off between bandwidth and sensitivity must be considered depending on specific applications.

2.5 ELECTRICAL MATCHING

Maximizing energy transmission and/or bandwidth can also be achieved by matching the electrical characteristics of the transducer to the electrical source and amplifier. Circuit components may be placed between the transducer and external electrical. The reactive part of impedance could be tuned out by adding an inductor either in series or in parallel with the transducer[6], [7].

2.6 Losses in Piezoelectric Materials

In general, in piezoelectric materials two kinds of losses can be distinguished: mechanical and dielectric. These losses can be taken into account by replacing elastic and dielectric constants with their complex values [22]. In other words, the mechanical and dielectric losses are taken into account by using complex elastic constant $\boldsymbol{C}_{33}^{\boldsymbol{E}*}$ and complex dielectric constant $\varepsilon_{33}^{\boldsymbol{E}*}$, respectively. These complex constants can be written as:

$$C_{33}^{E*} = \boldsymbol{C_r} + \boldsymbol{jC_i} = \boldsymbol{C}_{33}^{\boldsymbol{E}}(1 + \boldsymbol{j}\delta_{\boldsymbol{m}}) \qquad (2.9)$$

$$\varepsilon_{33}^{S*} = \varepsilon_{\boldsymbol{r}} - \boldsymbol{j}\varepsilon_{\boldsymbol{i}} = \varepsilon_{33}^{\boldsymbol{S}}(1 - \boldsymbol{j}\delta_{\boldsymbol{e}}) \qquad (2.10)$$

where the subscripts r and j stand for real and imaginary terms. $\delta_{\boldsymbol{m}}$, $\delta_{\boldsymbol{e}}$ are the mechanical and dielectric losses, respectively.

2.7 ARRAYS

Arrays transducers involve more than one element. These elements may be rectangular-shaped and arranged in a line (called one-dimensional linear array transducer); square in shape and arranged in rows and columns (called two-dimensional array transducer); or ring shaped and arranged concentrically (called annular array). The schematic diagram of a linear array transducer is shown in Figure 2.4. Compared to the single-element transducers, array transducers have been widely utilized in many clinical applications due to their clinical convenience, increased frame rates and the capability to focus the beam dynamically [15]. An array is operated by applying successively voltage pulses to groups of elements. The sound beam is moved across the face of the transducer electronically, producing an image similar to the case obtained by scanning a single transducer mechanically [16].

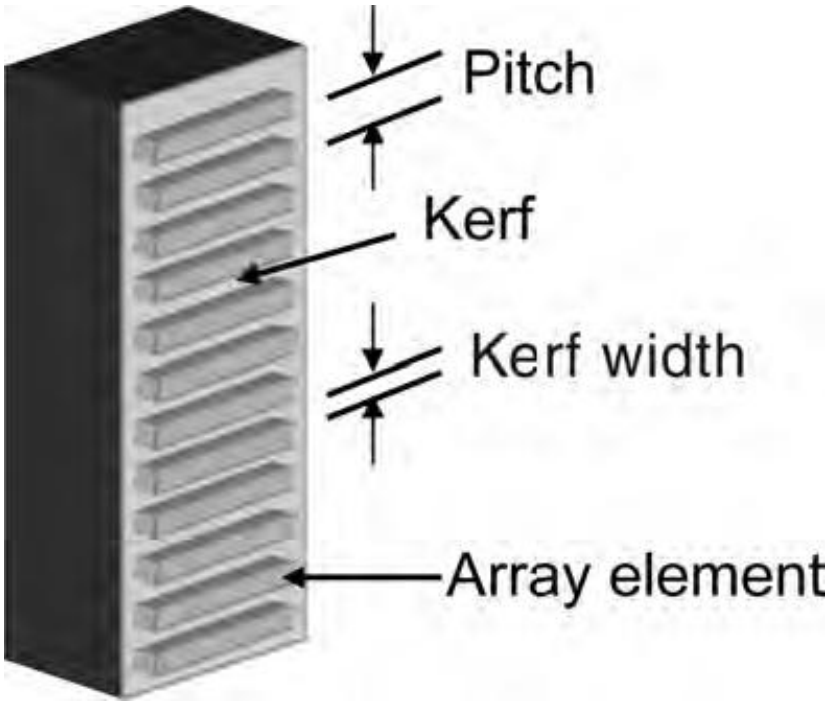

Figure 2.4: Schematic diagram of array transducer [12]

In the most basic sense, a phased array system utilizes the wave physics principle of phasing, varying the time between a series of outgoing ultrasonic pulses in such a way that the individual wave fronts generated by each element in the array combine with each other to add or cancel energy in predictable ways that effectively steer and shape the sound beam.

The returning echoes are received by the various elements or groups of elements and time-shifted as necessary to compensate for varying acoustic lens and then summed. Unlike a conventional

single element transducer, which will effectively merge the effects of all beam components that strike its area, a phased array transducer can spatially sort the returning wave front according to the arrival time and amplitude at each element. When processed by instrument software, each returned focal law represents the reflection from a particular angular component of the beam, a particular point along a linear path, and/or a reflection from a particular focal depth. The echo information can then be displayed in any of several formats. Compared to the single-element transducers, array transducers have been widely utilized in many clinical applications due to their clinical convenience, increased frame rates and the capability to focus the beam dynamically [10]. The sound beam is moved across the face of the transducer electronically, producing an image similar to the case obtained by scanning a single transducer mechanically [11].

2.8 Modeling of transducer

Modeling plays an important role in the development of a new transducer. A reliable model provides prior prediction of a transducer behavior and its performance. In this case, the electro acoustic properties. New transducers can be designed and optimized before moving to the fabrication step based on modeling. In this thesis, modeling of the transducers consists of analytical one dimensional (1D) models and 3D FEM simulations of the electro-acoustic behavior, and simulations of the beam shape using Field II.

2.8.1 One-dimensional model

In many cases, a 1D equivalent circuit model is sufficient to describe the thickness vibrations mode of the piezoelectric transducer. There are many other existing current models, but the most used are the Mason, Redwood and Krimholtz, Leedom and Matthaei (KLM) models. In this research, the Mason model is used, implemented in the XTrans program, and the KLM model, implemented in peizocade.

2.8.2 FEM Simulation

Finite element method (FEM) is a general simulation technique to approximately solve partial differential equations in physics, mechanics, chemistry, or biology problems. It has been used to model a transducer's behavior, especially when simple 1D model is not able to predict the performance of the transducer. A 1D model can only investigate vibrations in one-dimension. The model assumes that the thickness of the backing layer is semi-infinite without losses [25].This means that any acoustic wave transmitted to the back does not reflect back from other interfaces. In reality, these reflections can interfere with the received echo from the front side, if the backing layer has less attenuation. The model is made for a piezoelectric material having the lateral dimensions much larger than the thickness. In practice, due to space limitations, the piezoelectric seldom satisfies these geometrical constraints. Consequently, the model results will become unreliable and less accurate. The model is made for a thin, loss-less, disc shaped piezoelectric material. It is not valid for a lossy piezo ceramic and polymer based piezo element.A finite element model for an ultrasonic transducer provides a realistic transducer simulation and gives a way to visualize the real acoustic wave propagation into the acoustic medium [26].Using the finite element method, we can cope with all the limitations described above for one-dimensional model. Using the finite element model a three-dimensional pressure field can be investigated. Finite element models are based on the governing equations of the acoustic propagation and piezoelectricity, so back reflections from any interface can be modeled and investigated. With the 3D or 2D axisymmetric models, we can simulate all the vibration modes upon the excitation of a piezo crystal layer. There is no geometrical constraint for accurate simulations. The losses in the materials (both in active and passive materials) can be modeled easily by setting the appropriate material properties. The interaction of the acoustic field of an ultrasonic transducer with other objects can be simulated. Besides the above advantages, finite element modeling has certain disadvantages as well. In order to obtain required accuracy at high frequencies, the finite element model of an ultrasonic transducer comprises of several thousands to few million degrees of freedom. Such a large model requires computer systems with extensive processing capabilities and considerable effort to build debug and operate. Another disadvantage of finite element modeling is that the response of a transducer can differ substantially from the actual response.This can be due to the use of an inadequate number of elements to resolve acoustic waves, unrealistic boundary conditions or less precise model

parameters (such as material properties). These drawbacks indicate the need for experimental validation of a finite element model. With this technique, the piezoelectric transducer and its surrounding medium are divided into a one, two or three-dimensional mesh of elements. The electric potential and elastic vibrations are computed from finite element matrix equations [8].The finite element equations are solved at each node in the mesh and at frequency range.

2.8.3 Fundamental piezoelectric theory

The constitutive equations for a piezoelectric material are given by:

$$T = [c^E]\, S - [e]^t\, E \tag{2.11}$$

$$D = [e]\, S + [\varepsilon^S]\, E \tag{2.12}$$

In 3D case,T is the 6x1 stress vector, c is 6x6 the elasticity matrix, S is the 6x1 strain vector, e is the 3x6 piezoelectric matrix, E is the 3x1 electric field vector, D is the 3x1 electric displacement vector, and ε is the 3x3 dielectric permittivity matrix,$[e]^t$is the transpose of $[e]$. The superscripts *E*, *S* indicates a zero or constant corresponding field [9].

When these matrices are provided in a modeling configuration, COMSOL recognizes which equations to be applied to each specific domain in FEM models. The electrical impedance Z of a piezoelectric element can be expressed by the following formula:

$$Z = \frac{V}{I} \tag{2.13}$$

Where V is the potential difference voltage across the two piezoelectric material faces and I is the current flowing inside.

The electric current flowing in the element can be calculated by the following integral:

$$I = b\int_0^d j_y\, dx \tag{2.14}$$

Where $j_y$the current density component along y axis, d is is the piezoelectric material width, b is the length of each element [9]. Material data used the simulations are given in Table. 1.2D Finite

Element Method (FEM) simulations were performed using COMSOL Multiphysics version 5.2a.

$$\nabla^2 p(r,t) - \frac{1}{c^2}\frac{\partial^2 p(r,t)}{\partial t^2} = 0 \qquad (2.15)$$

Where $p(r, t)$ is the pressure and c is the speed of sound in the medium [9].

It is possible to identify two significant regions where wave propagation characteristics are very different: near field and far field region [10]. As regard our application, the region of interest is generally the far field, where waves are locally planar and the pressure amplitude drops at a rate inversely proportional to the distance from the source.

3 CHAPTER METHODS

In this chapter fabrication of high frequency transducer array and low frequency transducer array are described and it also contains how to combine them to make a dual frequency transducer array. Fabrication of high frequency transducer array was completed in University of Southern California Los Angeles (USC) and the fabrication method described below is taken from the ultrasound lab situated in USC.

3.1 Fabrication process of high frequency transducer array

The high frequency transducer array was fabricated using fuji c-82 as a pzt material and two matching layer on top of it. Firstly, the PZT material was attached to the glass and first matching layer i.e. 2-3 silver epoxy was deposited on top of it. After getting the final thickness of first matching layer by lapping, the sample was diced into array and fills the kerf with epotek and cured it for 3 days under room temperature. Finally the second matching layer i.e. parylene was deposited on top of the first matching layer.

The very detailed description of the fabrication process is presented below.

3.1.1 Piece of glass selection

Piece of glass was selected. To check the variation in thickness HEIDENHAIN thickness gage was used, suction turn on to check the rainbow pattern. To find the glass is fine or not you need to push down on the corners, if rainbow pattern moves a lot then try the other side of the glass. If the rainbow pattern now does not move much, then this side is good to work on. Zero the instrument to make sure the glass is parallel. For this purpose, measured thicknesses at different points on the glass must be the same. There should not be more than 4 to 5 um variation in thickness of the piece of glass.

3.1.2 Sandpaper station

Edges of the piece of glass were scraped to avoid sharp edges on the sand paper. Firstly start with the large edges and then continue with the corners. Now, mechanical cleaning was performed on the glass with acetone, alcohol and di-water respectively to remove the dust particle.

3.1.3 Piezoelectric sample wax bonded to piece of glass

Stacking fixture base and top were Placed on the THERMOLYNE hot plate to start warming them up. The temperature of hot plate was set at 60^0 to 65^0C. I Select a piece of rubber and another piece of glass and did the mechanical cleaning for both of them. I stick the piece of rubber to the piece of glass and added one piece of Mylar to the rubber + glass set. Now the placement of Mylar + rubber + glass set and the previous piece of glass with scraped corners separately on the hot plate to warm them was done. Next step was to place the piezoelectric (ceramic) i.e. Fuji c-82(Fuji Ceramics Co. Ltd. Japan) on top of the glass with scraped corners and add 60 C-wax from only one end of the ceramic to surround it. If wax is added from more ends, it's easy to trap bubbles. To get rid of the bubbles we need to press the ceramic. This practice becomes even more important when dealing with composites. The ceramic was covered with a piece of Mylar. Take a tissue (kimwipe) and fold it to a 2" x 2" square. Stacking everything together was done as shown Figure 3.1 and the stack was covered with the fixture top. The whole stacked was placed inside the oven (Fisher Scientific Isotemp Oven) for around 30 minutes at 60^0 to 65^0C. The wax will stay in liquid state. This will also help it distribute more uniformly across the glass. After the time has elapsed, the stack was taken out of the oven and allows it cool down for about 15 to 20 minutes. Next step was to check if there are some bubbles or not if there are, heat up again to get rid of them and check back again. Now, cleaning was done to remove the excess of wax. For wax close to the edges of the ceramic a razor blade was used. By using a fine-point foam swab with trichloroethylene to completely remove wax close to the ceramic edges. At the end, cotton swabs were used with acetone and then alcohol for mechanical cleaning.

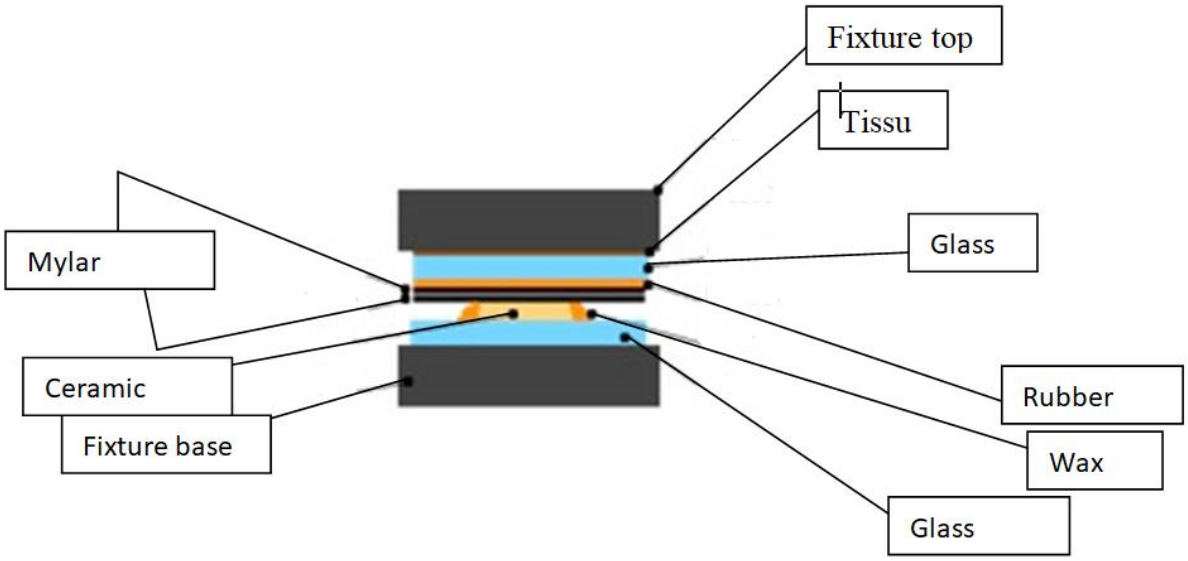

Figure 3.1: Stacking order to attach the ceramic and glass.

3.1.4 Spacer placement on piece of glass with piezoelectric sample

The spacer's was cut by using PRAZI SD 400 lathe. 1-mm thick spacers were required. By using the sandpaper 1500 to scrape the newly machined spacers and make them flat. After cleaning I gave them numbers and that helped me a lot while lapping. Now, glue them with LOCTITE 454 to the scraped corners of the piece of glass with the piezoelectric ceramic. The numbers must be facing down.

3.1.5 Piezoelectric 1st side lapping

The piezoelectric thickness is not critical for the first side lapping. For the first side to lap, I started with wet sandpaper #400 to get the spacers to the same thickness as the piezoelectric sample. Once they all have the same thickness, I switched to wet sandpaper #1500. To ensure uniform lapping our hand follows "8-shaped" trajectories. At the end, aluminum oxide powder was used on the wet sandpaper to avoid scratching the piezoelectric piece and lapping was done to matte finish. After lapping the first side to matte finish, mechanical cleaning was performed on the piece of glass using a cotton swab with acetone followed by alcohol.

3.1.6 Electroplating sputtering

At first mechanical cleaning was performed and then the sample was prepared for gold sputtering using NSC 3000 Automatic sputter coater. The piece of glass was masked using Kapton masking tape. The masked piece of glass with the recently cleaned piezoelectric should look like that shown in figure 3.2. Notice that the sides of the piece of glass are masked too and only the piezoelectric piece is exposed. Side view is shown in figure 3.3

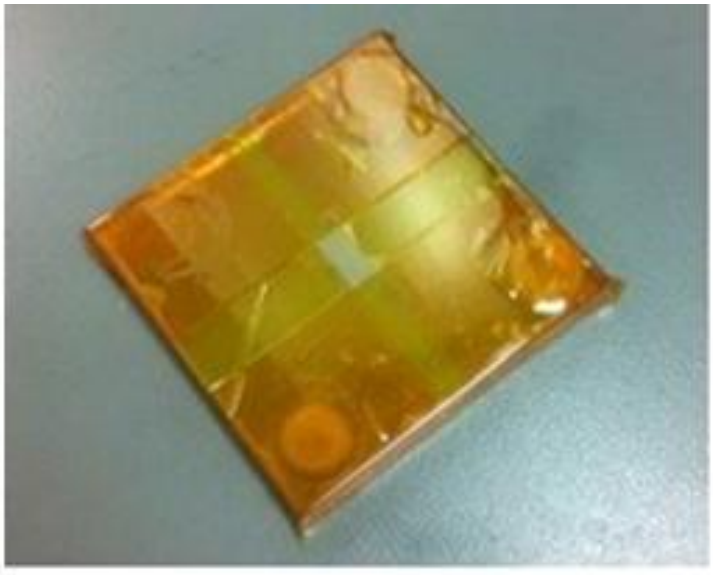

Figure 3.2:Masked piece of glass with piezoelectric material.

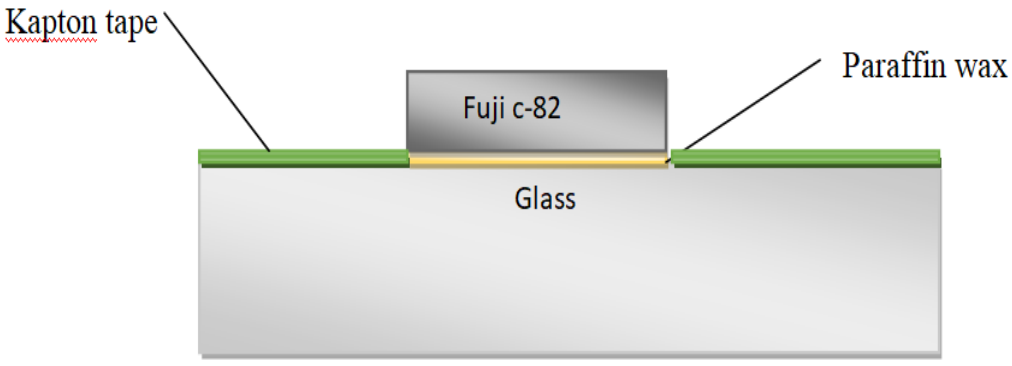

Figure 3.3:Masked piece of glass with piezoelectric material side view.

The piezoelectric sample comes out with a sputtered coating of chrome 500 Å and gold 1000 Å. The sample after sputtering look like that shown in Figure 3.4 and its side view is shown in figure 3.5.

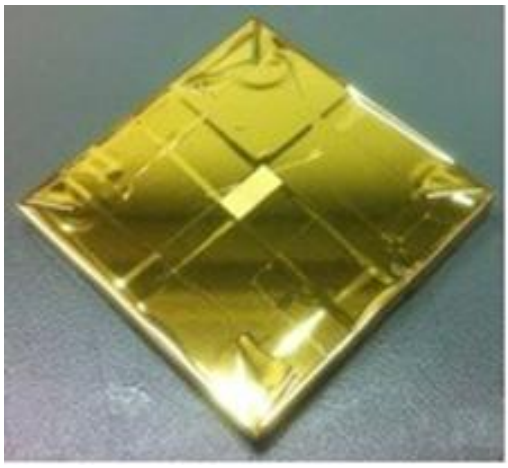

Figure 3.4:Masked piece of glass with piezoelectric after sputtering.

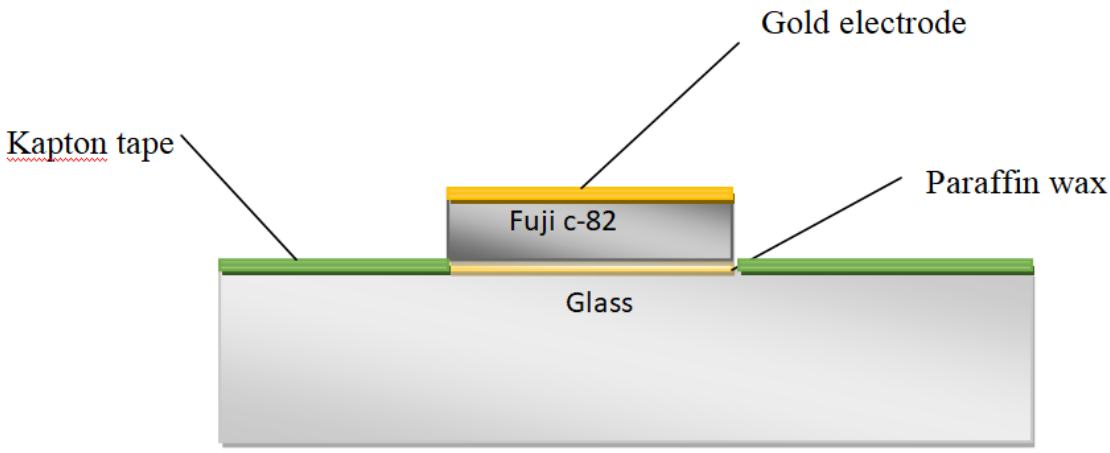

Figure 3.5:Masked piece of glass with piezoelectric after sputtering side view.

3.1.7 Placing new spacers and the dam for matching layer

The piece of glass was unmasked by carefully removing the Kapton masking tape. The spacers were removed from the glass. I Use razor blade for this purpose and with a cotton swab cleaning of the glass was performed with acetone followed by alcohol. Next step was to mix 5-minute epoxy in a small plastic tray and apply it with a toothpick or a fine-point foam swab close to

the external edges of the dam. This will prevent the epoxy from getting inside the dam and eventually contacting the piezoelectric sample. The dam was placed on the glass in such manner so that the piezoelectric sample is surrounded by it. Now, new four spacers were diced using lathe machine, number the spacers was done, and gluing them to the glass in was done. The piece of glass with the new spacers and the sputtered piezoelectric surrounded by the dam should look like that shown in Figure 3.6.

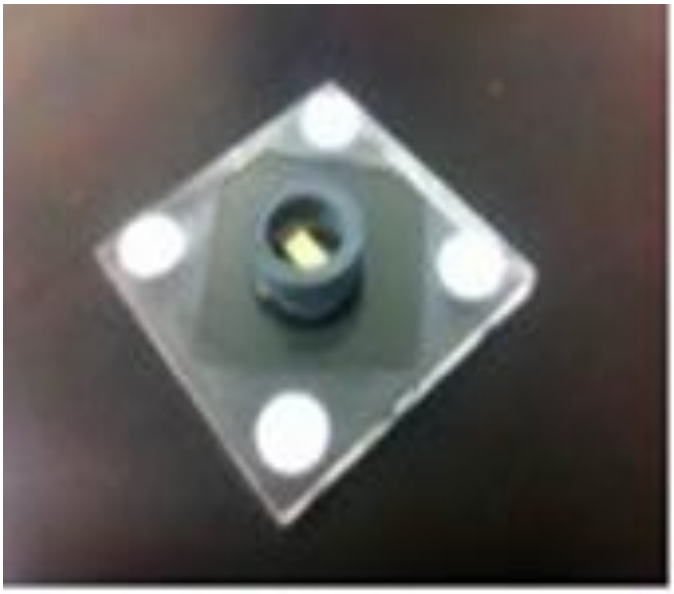

Figure 3.6:The piece of glass with the new spacers and the sputtered piezoelectric surrounded by the dam

3.1.8 Preparing and casting 1st matching layer

The plasma cleaning was done by authorized person for 15 minutes. Before hand in the sample the thickness of sample was measured, it helped to find the exact thickness of matching layer. Next step was to spray AP13 in isopropanol (0.5% solution) over the sputtered piezoelectric sample o make it more adhesive. The purpose of AP131 in isopropanol is to promote the adhesion of silver epoxy to gold. Let it cure in air for approximately 30 minutes. While the AP131 in isopropanol was curing, preparation of 2-3 um silver epoxy was done which was used as the 1st matching layer (Adrich Chem. Co., Milwaukee, WI) [16], [17]. To do so we start by mixing Insulcast 501 with Insulcure 9 (Americal Safety Tech., Roseland, NJ). This mixture

was the epoxy. In a small plastic beaker, 10 gr. of Insulcast 501 for every 1.3 gr. of Insulcure 9 was purred. For the present transducer design, 4 gr. of Insulcast 501 and the corresponding 0.52 gr. of Insulcure 9 are enough for 5 transducers. Use the OHAUS Adventurer digital laboratory scale for weight measurements. With a plastic lab spatula, the epoxy mixture was mixed for approximately 10 minutes to incorporate both substances uniformly. Afterwards, in a small plastic tray 2-3 um Silver powder was added. 3 gram of 2-3 um silver powder for every 1.25 gr. of epoxy mixture was used. 2-3 um silver powder was added to the epoxy mixture and by using the same plastic lab spatula, everything was mixed together for approximately 10 to 15 minutes. Now that the AP131 in isopropanol has cured, carefully casting of the 2-3 um silver epoxy on top of the sputtered piezoelectric sample was done. Stirring stick was used for this purpose. The sample was placed inside one of the bottles of the BECKMAN COULTER Allegra 6 Centrifuge machine. Sample was centrifuge at 3,000 rpm for approximately 15 minutes. After centrifuging time is over, Notice how the 2-3 um silver epoxy is now uniformly distributed. After centrifuging of the sample was placed in drying box and the 2-3 um silver epoxy dried in overnight. The sample was placed inside the oven to post-cure 2-3 um silver epoxy for 2 hours at 45 °C. Lapping the cured 2-3 um Silver epoxy to final design thickness as described earlier was done. After lapping, with a cotton swab mechanical cleaning of the piece of glass with acetone followed by alcohol was done. The sample with the 1st matching layer lapped to final design thickness should look like that shown in Figure 3.7 and its side view is shown in figure 3.8.

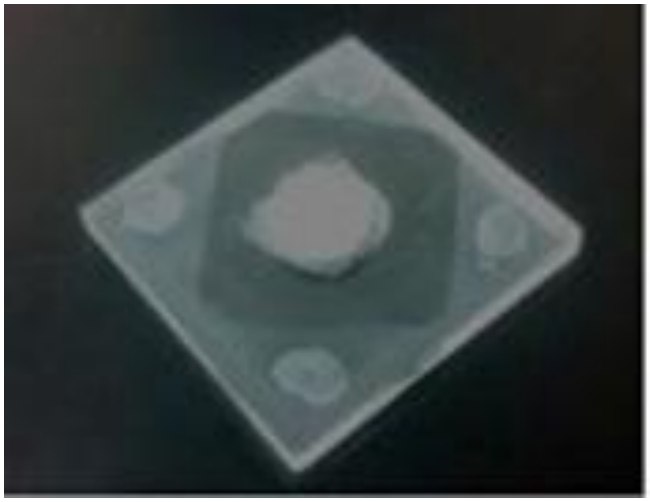

Figure 3.7:The sample with the 1st matching layer lapped to final design thickness

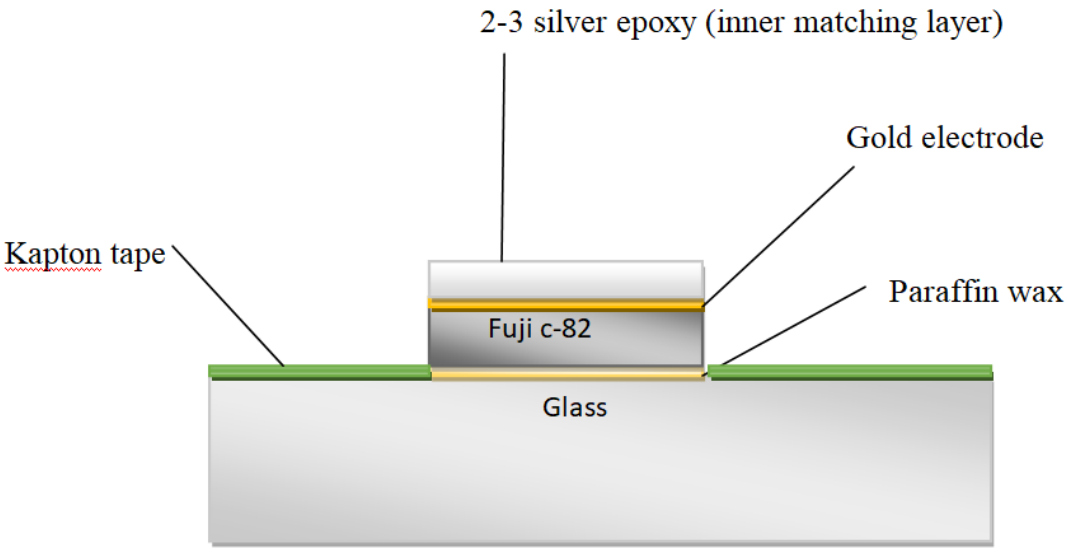

Figure 3.8: The sample with the 1st matching layer lapped to final design thickness side view.

The sample was prepared for dicing by drawing lines to mark its position. For this purpose I use the Nikon microscope to help on this step. I put my sample upside down on a kimwipe or a lint-free paper piece and center it exactly under the microscope view so that my eyes are not looking

at it from an angle, but rather from its very top. With a marker and a ruler, lines were drawn from left to right. After drawing the four lines that denote the position of the piezoelectric sample, the lines were covered with Kapton or Teflon masking tape. The sample should look like that shown in Figure 3.9. Now, the dicing of the sample by using Thermo carbon, Inc. Tcar 864-1 Programmable Dicing Saw with SmartGrafix has been done. Then, the sample was removed from the glass and attached to the new glass in similar manner.

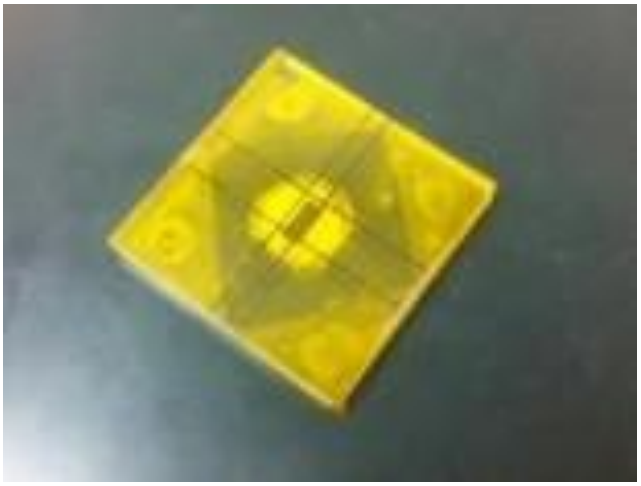

Figure 3.9: Prepared sample for dicing

3.1.9 Arrays formation

Once the piezoelectric sample wax bonded to the piece of glass it was diced into 350 cuts with us H405RM - T4 – 013040 ASAHI Dicing Blades and Thermo carbon, Inc. Tcar 864-1 Programmable Dicing Saw with SmartGrafix with the specification of 80 um pitch and 15um kerf. Now, put the sample in di-water and leave it for one night followed by ultrasonic bath for the cleaning. Each and every kerf was tested under microscope whether it is clean or not. To fill the kerf Epotex 4:1 epoxy (Epoxy Technologies, Billerica, MA) was used and mix both material for 2 minutes and then put it in the vacuum chamber to get rid of air bubble. Once the kerf has filled with epoxy put it back into the vacuum chamber to remove the air bubble and leave it for 3 days to cure in dry box at room temperature. Before lapping the epoxy from top of the sample

you need to put the sample in oven for 2 hours at 45^0C for post curing and then start lapping to expose the kerf.

Lapping was done because to get rid of epoxy from top of the sample and expose the kerf. For the first time to lap, I started with wet sandpaper #400 to get the spacers to the same thickness as the piezoelectric sample. Once they all have the same thickness, I switched to wet sandpaper #1500 and expose the kerf. Lapping was performed in a manner where hand follows "8-shaped" trajectories to ensure uniform lapping. Never let the sandpaper become dry. At the end, I added aluminum oxide powder on the wet sandpaper to avoid scratching the piezoelectric piece and lap to matte finish. Now, to get the final thickness first remove the sample from glass and fillip it over and again attach it to the glass in similar way as did before. Start lapping and expose the kerf from back be careful while lapping because it is going to be your final thickness. Once you reach the final thickness clean it with acetone followed by alcohol and di-water then sputtering the gold electrode on top of it. Now the transducer is ready to be diced in to final size in my case it is 5.6mm x 3mm. A 26-μm-thick parylene outer matching layer was then vapor deposited (PDS2010, Specialty Coating Systems, Indianapolis, IN) on top of the inner matching layer [16], [17]. Specification of the transducer and material properties is listed in Table 1 and Table 2 respectively. The whole fabrication process is shown in figure 3.10

1.Selection of glass

2. Bonding of peizo material to the glass with the help of paraffin wax.

3. Sputtering of gold electrode on top of the Peizo material.

4. Deposition of 2-3 silver epoxy (inner matching layer) on top of the piezo material and lap it down to the final thickness i.e. 20um.

5. Array formation and filling the array with E-potek. After curing it lap it down to the final thickness from bottom and second electrode sputtering.

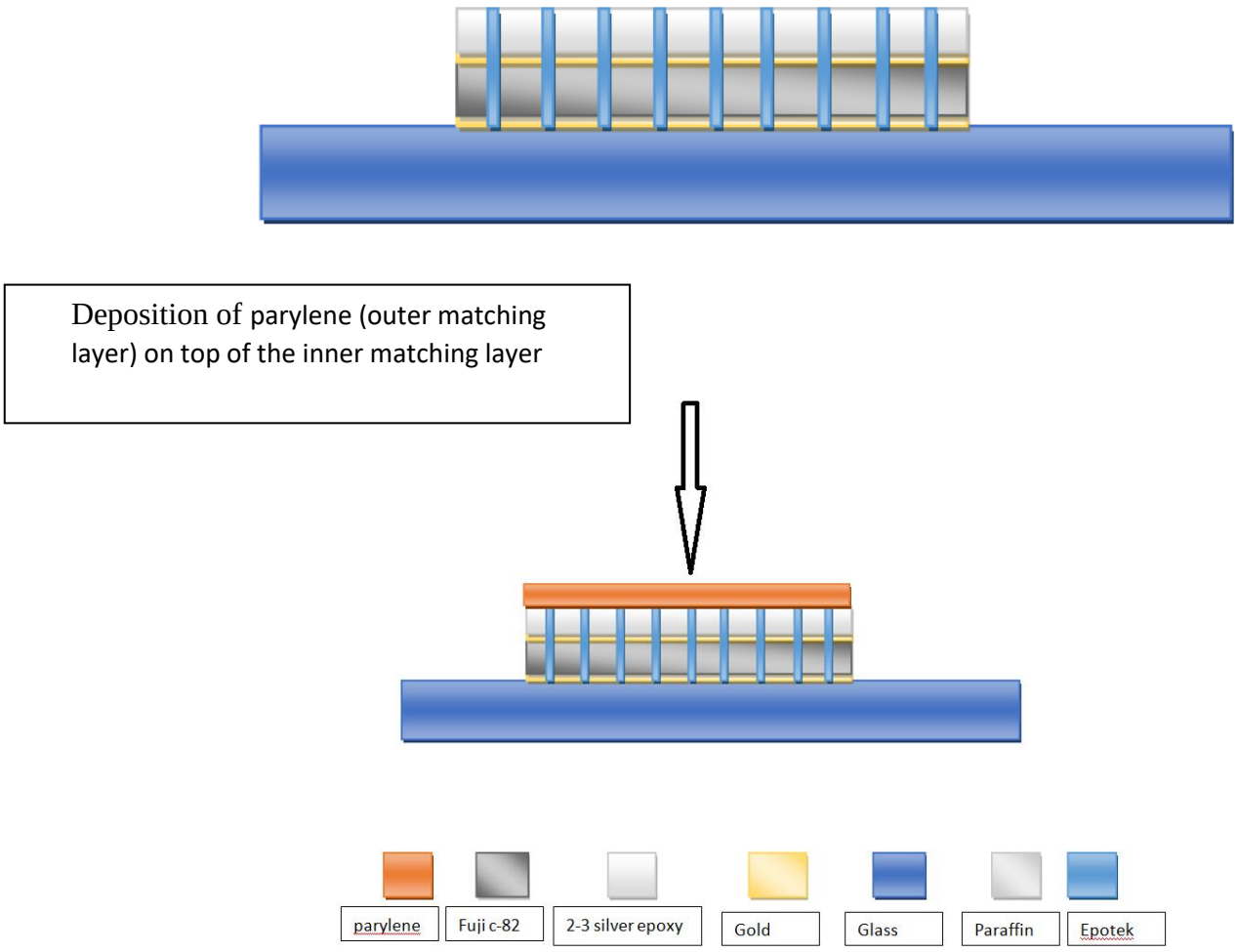

Figure 3.10: Fabrication process of high frequency transducer array

Table 1: Optimized parameters of the phased-array transducer 20 MHz.

Designed center frequency	20 MHz
Number of elements	64
Pitch	80 um
Elements width	65um
Elements length	3 mm
Azimuthal dimension	5.6 mm
Kerf width	15 um
Fuji C-82 thickness	80 um
First matching layer thickness	20 um
Second matching layer thickness	26 um

Table 2: Material specification for 20 MHz transducer array [[16], [17], [27].

	Material	Long. Velocity (m/s)	Density (kg/m^3)	Acoustic impedance (Mrayls)	Clamped dielectric constant (e_{33}^s)	Electromechanical coupling coefficient (k_t)	Q value
PZT	Fuji c-82	4027	7400	29.8	1259	0.76	76
Inner matching layer	2-3 micron silver	1900.0	3860	7.334			28
Outer matching layer	parylene	2350.0	1100	2.585			41

3.2 Finite Element Model

3.2.1 Finite Element Model of single element 20 MHz transducer

The piezo disk transducer's model was build using COMSOL Multiphysics 5.2a acoustic-piezoelectric interaction module in the frequency domain. This model is investigated in 2D model FEM COMSOL model is showed in detail in Figure 3.11. All these material are modeled in COMSOL as isotropic elastic materials, except for piezoelectric material shown in figure 3.12. A potential difference is applied to the top and bottom sides of the piezoelectric material to specify the electrical boundary condition. Mesh on all domains was chosen as free triangular with segment length less than approximately $\lambda/5$ to achieve acceptable compromise between accurate result and simulation time shown in figure 3.13. This model was build for 20 MHz transducer. Two matching layer was used on top of the piezo material.

Figure 3.11: COMSOL FEM Model for a single element transducer at 20 MHz

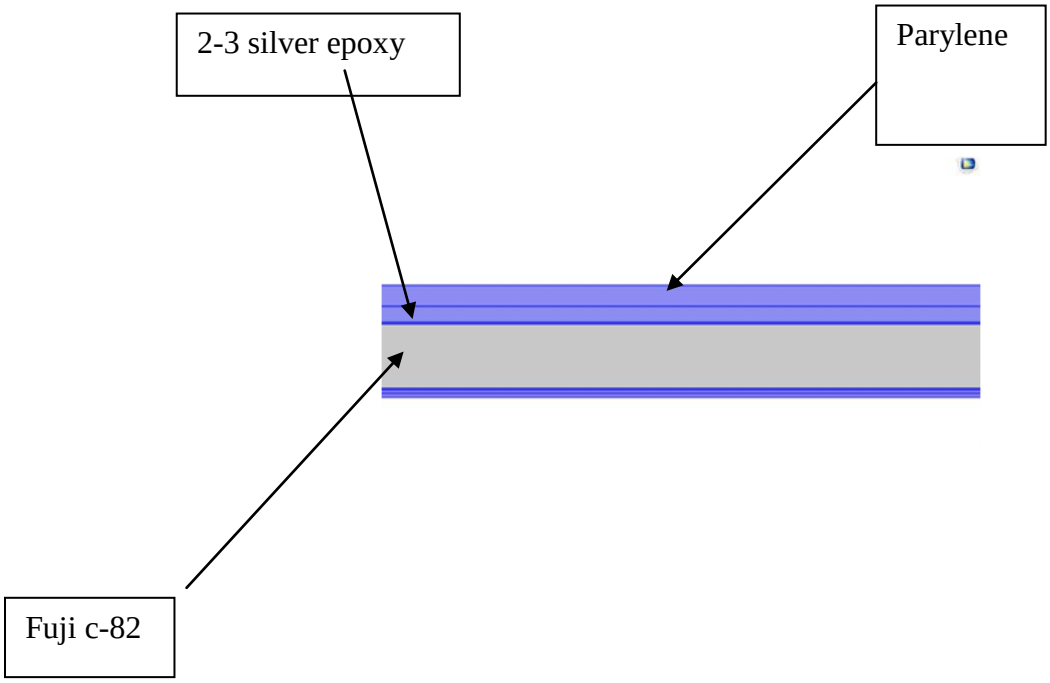

Figure 3.12:Isotropic elastic materials

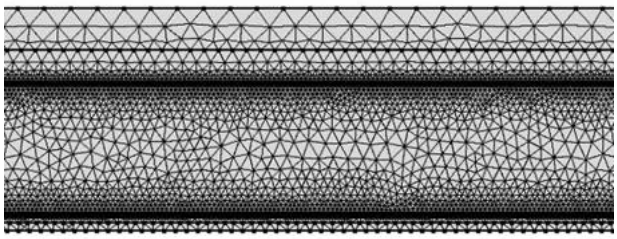

Figure 3.13: Optimization of mesh simulation

3.2.2 Finite Element Model of 20 MHz transducer array

The finite element model (FEM) was used to anticipate the performance of the matrix before manufacturing. The relevant properties of the active and passive materials used in the FEM model for 20 MHz transducer array are listed In Table 3 and Table 4. A finite element 2-D model using COMSOL was first used to generate an electrical impedance magnitude and a phase diagram of the set element. The array model is shown in figure 3.14. Mesh on all domains was chosen as free triangular with segment length less than approximately λ/5 to achieve acceptable compromise between accurate result and simulation time shown in figure 3.15.

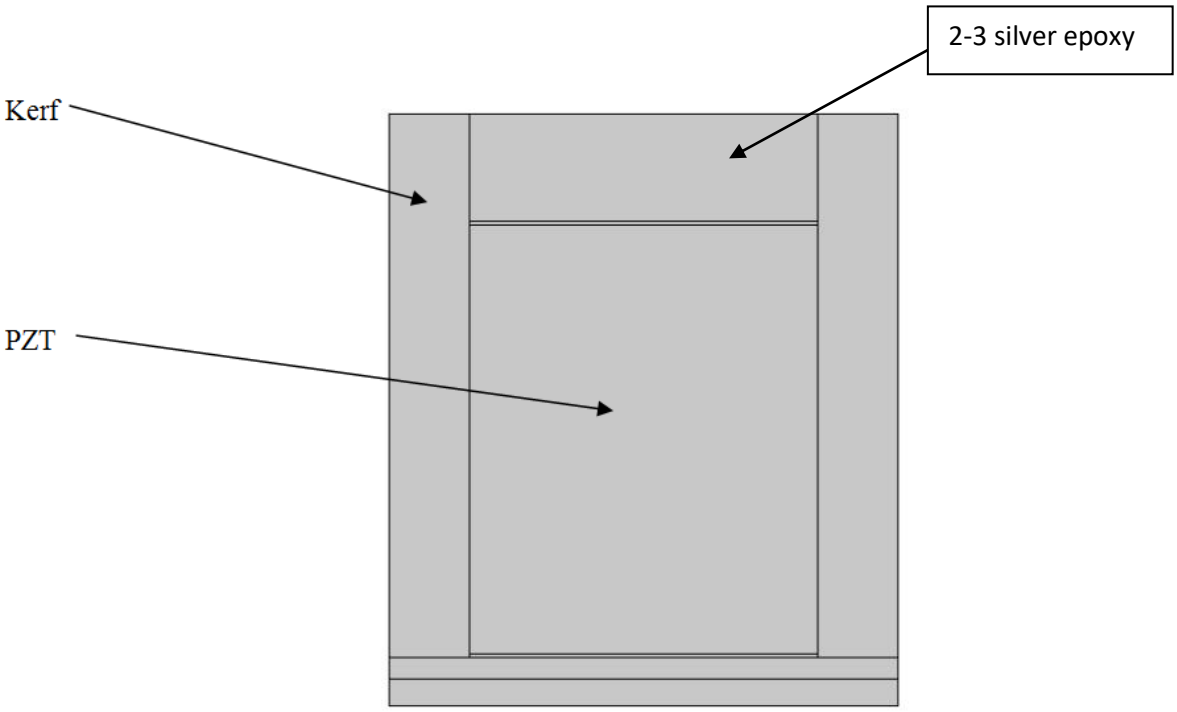

Figure 3.14: FEM model used in COMSOL for array element

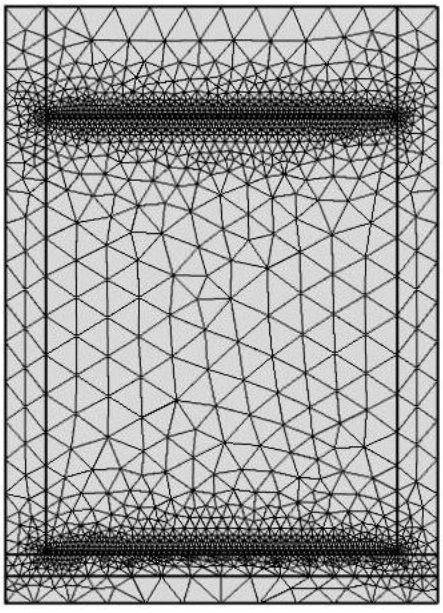

Figure 3.15: Optimization of mesh simulation

Table 3: Material data for fuji c-82 from Fuji Ceramics Co. Ltd. Japan [27].

Fuji c-82	Value
C_{11}^{E}[10^{10} N/ m^2]	13.8
C_{12}^{E}[10^{10} N/ m^2]	9.2
C_{13}^{E}[10^{10} N/ m^2]	9.1
C_{33}^{E}[10^{10} N/ m^2]	12
C_{44}^{E}[10^{10} N/ m^2]	2.2
C_{66}^{E}[10^{10} N/ m^2]	2.3
e31[C/ m^2]	-5.2
e33[C/ m^2]	26.5
e15[C/ m^2]	17.0
E_{11}^{S}/E_0	1540
E_{33}^{S}/E_0 (Epsilon)	1259
Kt	52.8
Density[kg/m^3]	7400

Table 4: Thickness values used in FEM Model for high frequency 20 MHz transducer array.

Piezo width [um]	Piezo thickness [um]	Upper electrode thickness [um]	Lower electrode thickness [um]	Cu thickness [um]	2-3 silver epoxy thickness [um]	Parylene thickness [um]	Bond thickness [um]
65	80	0.7	0.7	5	20	26	4

The FEM for array ultrasonic transduction was constructed using COMSOL Multiphysics 5.2a acoustic-piezoelectric interaction module in the frequency domain. This model is investigated in two dimensional spaces (2D). The results of the measurements were verified by the COMSOL model under the Acoustic-Piezoelectric Interaction Physics Package with the following boundary condition: periodic boundary condition was applied on the kerf and rest of the structure is free the electrical potential and the ground are applied to the lower and upper sides of the material piezoelectric. In order to visualize the characteristics of the vibration mode, we can check the animation of deformed form at a fixed frequency. The vibration was obtained by plotting the displacement field.

The electrical impedance of array transducer is given by:

$$Z = \frac{V}{I} \qquad 3.1$$

Where V is the potential difference voltage across the two piezoelectric material faces and I is the current flowing inside.

The electric current following in the element is given by:

$$I = b * \int_0^d j dx \qquad 3.2$$

Where ***j*** is the current density component along y axis, d is the piezoelectric material width, b is the length of each element. In this case, b = 3 mm.

3.3 Fabrication of 4 Mhz Transducer Arrays

The fabrication process of low frequency transducer array is described under this topic.

Piezoelectric material Pz27 used in the experiment was manufactured from Ferroperm A/S [18]. First we dice rectangular 5.6 x 3 mm^2 sample from circular sample by using Diamond blade (Z09-SD1700-Y1-60 53.4x0.033ASx40). Dicing step was performed by using DAD 321 dicing saw (Disco Corp., Tokyo, Japan). Now, we prepare the backing material. Firstly the material was lapped by using #400 sand paper followed by #1500 on MultiPrep system for grinding/polishing Allied (8030) purpose of lapping was to make the material flat. Pz27, Copper, and backing material were clean by using ethanol (baking material only) for 5 minutes in ultrasonic bath (Ultrasonic Cleaning Brandson (3100)) at 60^0c rinse off with running water for 30 seconds, after that put all the material in 2% soap (mix 2% of micron 90 in tap water 2g/100g) leave it in ultrasonic bath chamber for 5 minutes followed by rinse off with running water for 30 seconds, Now, back to back Di-water (de-ionized water) cleaning for 3 minutes, at the end isopropanol cleaning for 5 minutes and baked at 60^0 C in oven Thermal Chamber Thermaks TS4115 (2040) for 3h.

Pz27, Copper, and backing material were attached together by DP460 (3M, Scotch-Weld, Epoxy Adhesive), a bonding material used to stack up components. Degas process was performed in 3 minutes to sufficiently remove air bubble inside the epoxy because air bubble might prevent the ultrasound beam from transmitting into the medium. Applying uniform pressure to make sure that the bonding thickness is as thin and flat as possible. Curing the epoxy in the oven at 60^0 C for 3h was performed.

The next step was consequently to dice the sample into elements. Diamond blade (Z09-SD1700-Y1-60 53.4x0.033ASx40) was used in this test. Dicing step was performed by using DAD 321 dicing saw (Disco Corp., Tokyo, Japan). The specification of 4 Mhz transducer and material parameters are given in Table 5 and Table 6 respectively. After the dicing transducer was cleaned by ultrasonic bath and backed at 60^0 C in oven for 3h. Kerfs were filled with spurr's epoxy [28]. It is a mixture of four component and they are ERL4206- vinyl cyclohexene dioxide (VCD), DER 736- diglycidyl ether, NSA- nonenyl succinic anhydride, and DMAE-dimethylaminoethanol (s-1) and there ratio are 10g:6g:26g:0.4g respectively. Two grams of mixture is enough for a transducer. The mixture was degassed by putting them in to the vacuum chamber for 5 minutes to get rid of the air bubbles. Once the kerf was filled then the sample was placed in vacuum chamber again for 5 minutes to remove the air bubbles from kerf. Sample was cured in the oven for 7 hours at 60^0 C. The array's impedance was measured with a Network

Analyser 8753D (Network Analyser Hewlett Packard). Electrical probes made direct contact to each array elements. The whole fabrication process is shown in figure 3.16.

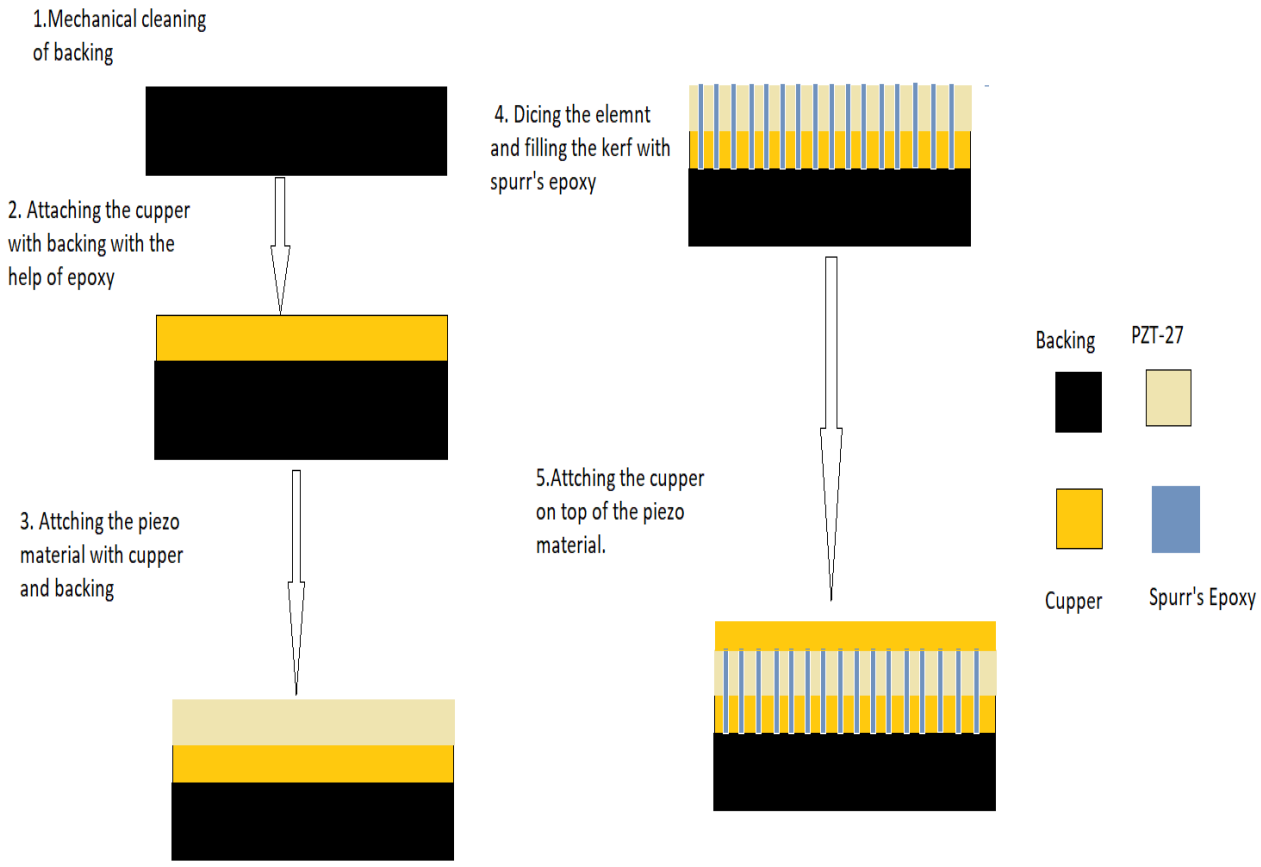

Figure 3.16: Fabrication process for low frequency transducer array.

Table 5: Parameters of the low frequency transducer array

Designed center frequency	4 MHz
Number of elements	23
Pitch	240 um
Elements width	207um
Elements length	3 mm
Azimuthal dimension	5.6 mm
Kerf width	33 um
Pzt-27	.524 um

Table 6: Material properties for 4 Mhz Transducer [24].

Layer	Material Properties					Thickness
	Coupling factor h(10^8V/m)	Dielectric constant S_r	Impedance Z (MRayl)	Velocity c (m/s)	Mechanical quality factor Q	T(mm)
Backing	-	-	4.5	-	6.25	.450
Piezoelectric	19.3	913	33.34	4330	74	0.5289
Bond line	-	-	2.8	2450	12.5	0.004
Copper	-	-	41.61	4800	30	0.006
MF110	-	-	3.5	2598	-	0.050

Dicing direction is shown in figure 3.17.

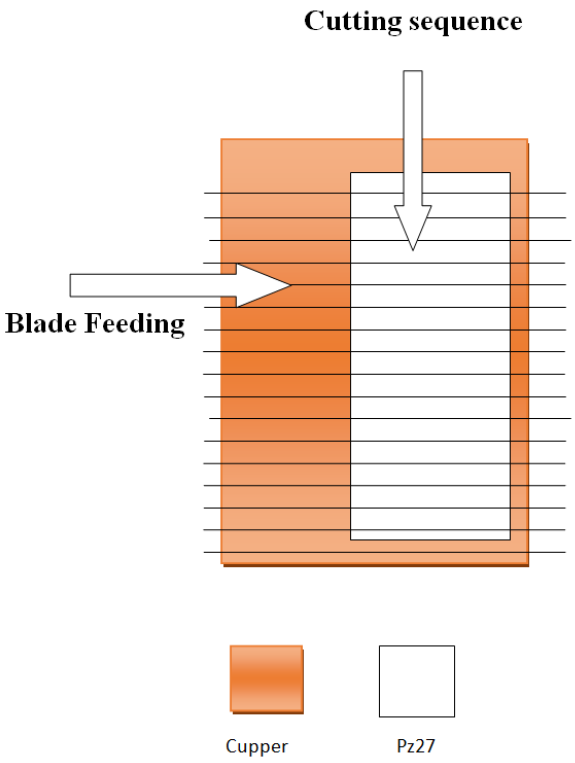

Figure 3.17: Cut direction.

‘Dicing parameters for the 4MHz transducer arrray’:

• Dicing blade: 0.033 mm thickness.

• Feeding speed: 1mm/s.

• Dicing height: 0.480 mm from the chuck.

• Pitch: 240 µm.

3.4 Finite Element Model

3.4.1 Finite Element Model of single element 4 MHz Transducer

The piezo disk transducer's model was build using COMSOL Multiphysics 5.2a acoustic-piezoelectric interaction module in the frequency domain. This model is investigated in 2D model FEM COMSOL model is showed in detail in Figure 3.18. All these material are modeled in COMSOL as isotropic elastic materials, except for piezoelectric material showed in figure 3.19. A potential difference is applied to the bottom and top sides of the piezoelectric material to specify the electrical boundary condition. Mesh on all domains was chosen as free triangular with segment length less than approximately λ/5 to achieve acceptable compromise between accurate result and simulation time shown in figure 3.20. There was no matching layer used for the 4 MHz transducer.

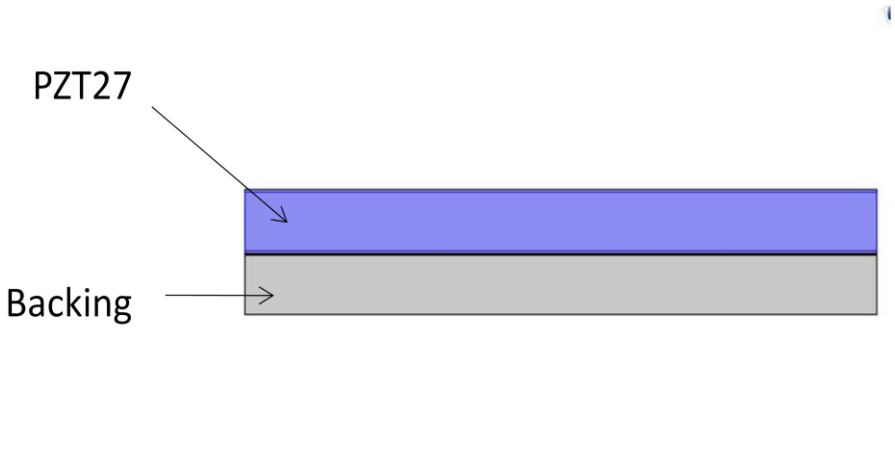

Figure 3.18:COMSOL FEM Model

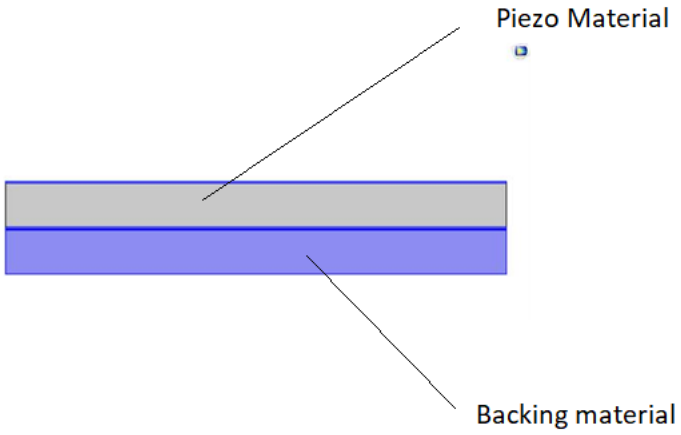

Figure 3.19: Isotropic elastic materials

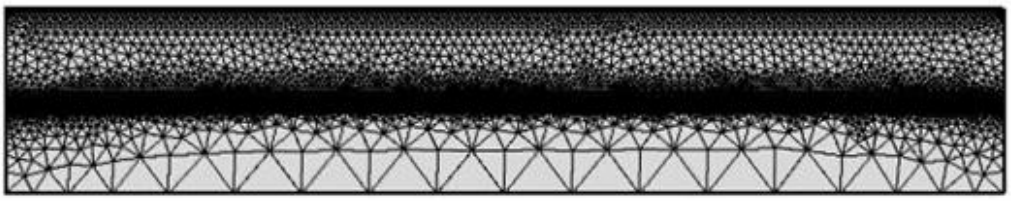

Figure 3.20: Optimization of mesh simulation

3.4.2 Finite Element Model of 4 MHz Transducer array

The finite element model (FEM) was used to anticipate the performance of the matrix before manufacturing. The relevant properties of the active and passive materials used in the FEM

model for 4 MHz transducer array are listed In Table 7 and Table 8. A finite element 2-D model using COMSOL was first used to generate an electrical impedance magnitude and a phase diagram of the set element. The model is shown in figure 3.21. Mesh on all domains was chosen as free triangular with segment length less than approximately λ/5 to achieve acceptable compromise between accurate result and simulation time shown in figure 3.22.

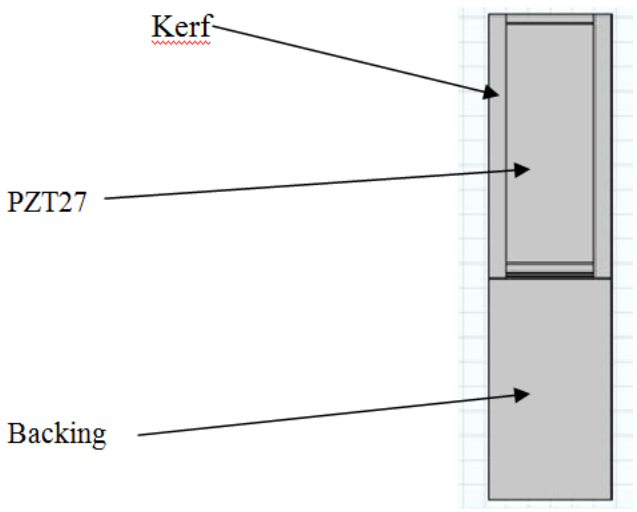

Figure 3.21: FEM model used in COMSOL for array element

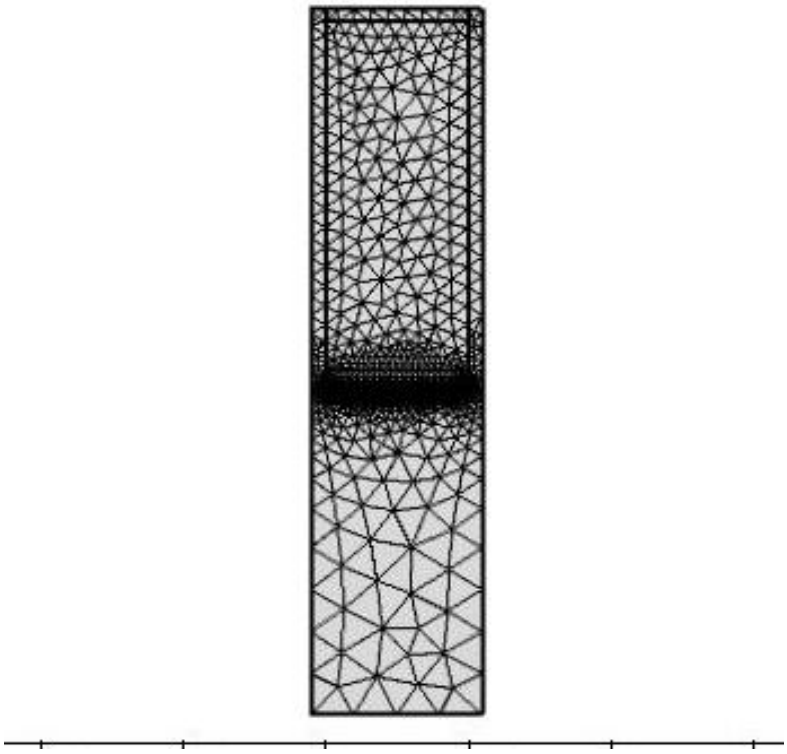

Figure 3.22:Optimization of mesh simulation

Table 7: Thickness values used in FEM Model

Piezo width [um]	Piezo thickness [um]	Upper electrode thickness [um]	Lower electrode thickness [um]	Cu thickness [um]	Bond thickness [um]
200	490	18	18	5	4

Table 8: Material data for Pz27 [24].

PZ27	Value
$\boldsymbol{C}_{11}^{\boldsymbol{E}}$[10^{10} N/ $\boldsymbol{m}^2$]	12.0 (1+i/110)
$\boldsymbol{C}_{12}^{\boldsymbol{E}}$[10^{10} N/ $\boldsymbol{m}^2$]	7.43 (1+i/250)
$\boldsymbol{C}_{13}^{\boldsymbol{E}}$[10^{10} N/ $\boldsymbol{m}^2$]	7.5 (1+i/200)
$\boldsymbol{C}_{33}^{\boldsymbol{E}}$[10^{10} N/ $\boldsymbol{m}^2$]	11.4 (1+i/177.99)
$\boldsymbol{C}_{44}^{\boldsymbol{E}}$[10^{10} N/ $\boldsymbol{m}^2$]	2.105 (1+i/75)
$\boldsymbol{C}_{66}^{\boldsymbol{E}}$[10^{10} N/ $\boldsymbol{m}^2$]	-
$^{\boldsymbol{e}}$31[C/ $\boldsymbol{m}^2$]	-5.4 (1-i/70)
$^{\boldsymbol{e}}$33[C/ $\boldsymbol{m}^2$]	16.0389 (1-i/200)
$^{\boldsymbol{e}}$15[C/ $\boldsymbol{m}^2$]	11.0 (1-i/200)
$\boldsymbol{E}_{11}^{\boldsymbol{S}}/\boldsymbol{E}_0$	916.02 (1-i/50)
$\boldsymbol{E}_{33}^{\boldsymbol{S}}/\boldsymbol{E}_0$ (Epsilon)	920.02 (1-i/80)
Kt	0.4658
Density[kg/m^3]	7700

The FEM for array ultrasonic transduction was constructed using COMSOL Multiphysics 5.2a acoustic-piezoelectric interaction module in the frequency domain. This model is investigated in two dimensional spaces (2D). The results of the measurements were verified by the COMSOL model under the Acoustic-Piezoelectric Interaction Physics Package with the following boundary condition: periodic boundary condition was applied on the kerf and rest of the structure is free, the electrical potential and the ground are applied to the upper and lower sides of the material piezoelectric. In order to visualize the characteristics of the vibration mode, we can check the animation of deformed form at a fixed frequency. The vibration was obtained by plotting the displacement field.

The electrical impedance of array transducer is given by:

$$Z = \frac{V}{I} \qquad 3.3$$

Where V is the potential difference voltage across the two piezoelectric material faces and I is the current flowing inside.

The electric current following in the element is given by:

$$I = b * \int_0^d j dx \qquad 3.4$$

Where ***j*** is the current density component along y axis, d is the piezoelectric material width, b is the length of each element. In this case, b = 3 mm.

3.5 Dual frequency transducer array

The low frequency (LF) layer was placed behind the high frequency (HF) layer (with respect to a forward-traveling sound wave) because low-frequency transmitted acoustic waves could propagate through the smaller, high-frequency element. The placement of the HF layer has little interference on the LF layer because of its small thickness (80μm) compared with the transmitting wavelength. The high-frequency layer was positioned in the front of the transducer to minimize the interference from the LF layer. A frequency-selective isolation layer with a quarter-wavelength of 20 MHz [19],[20] was placed between the two piezoelectric layers to allow the low-frequency transmitting wave to pass through, but the high-frequency receiving wave to be reflected at the isolation interface. The isolation section has two functions; preventing propagation of HF waves from the HF section into the LF section, and serving as an impedance matching structure for the LF section to the load [21]. The cross sectional overview of the stack is shown in figure 3.23. This is a general illustration of a two frequency stack. More detailed structure is shown in figure 3.24 with all layers. MF110 was used as an isolation layer (University College of southeast Norway). The material properties are given in table 6.

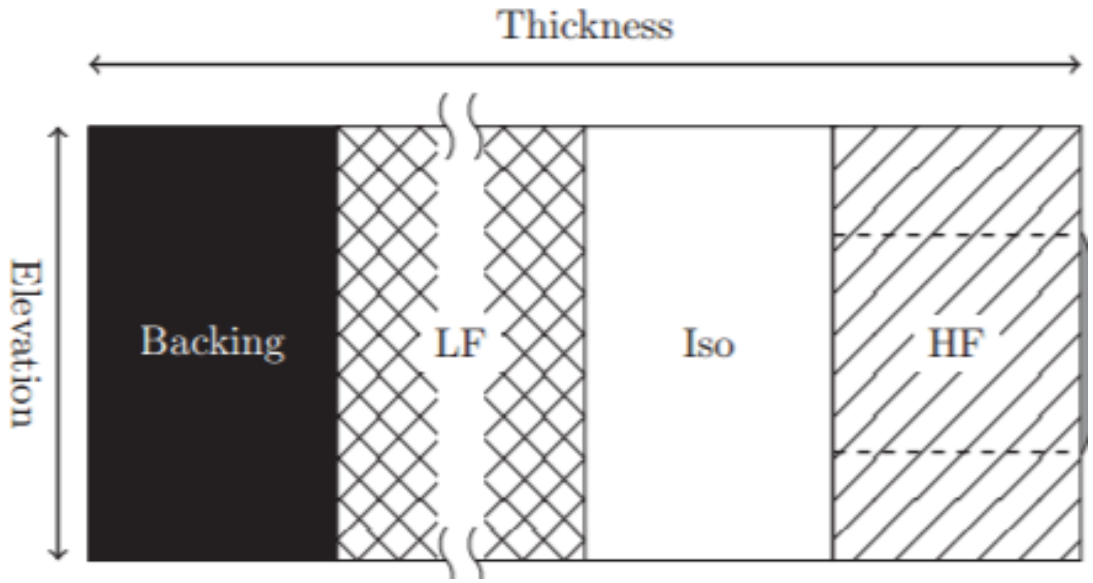

Figure 3.23: Cross-sectional overview of the stack structure, showing the different sections [21].

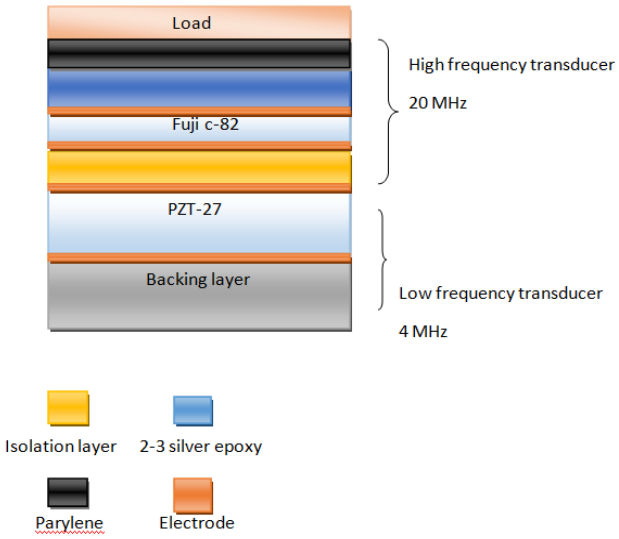

Figure 3.24: Side view of the structure of the two-frequency transducer stack, with one high frequency piezoelectric (Fuji c-82) and one low frequency (PZ27).

3.5.1 Finite Element Model

The finite element model (FEM) was used to anticipate the performance of the matrix before manufacturing. The relevant properties of the active and passive materials used in the FEM model for 4 MHz and 20 MHz transducer array are listed In Table 7, Table 8, Table 3 and table 4. A finite element 2-D model using COMSOL was first used to generate an electrical impedance magnitude and a phase diagram of the set element. The model is shown in figure 3.25. Mesh on all domains was chosen as free triangular with segment length less than approximately λ/5 to achieve acceptable compromise between accurate result and simulation time shown in figure 3.26.

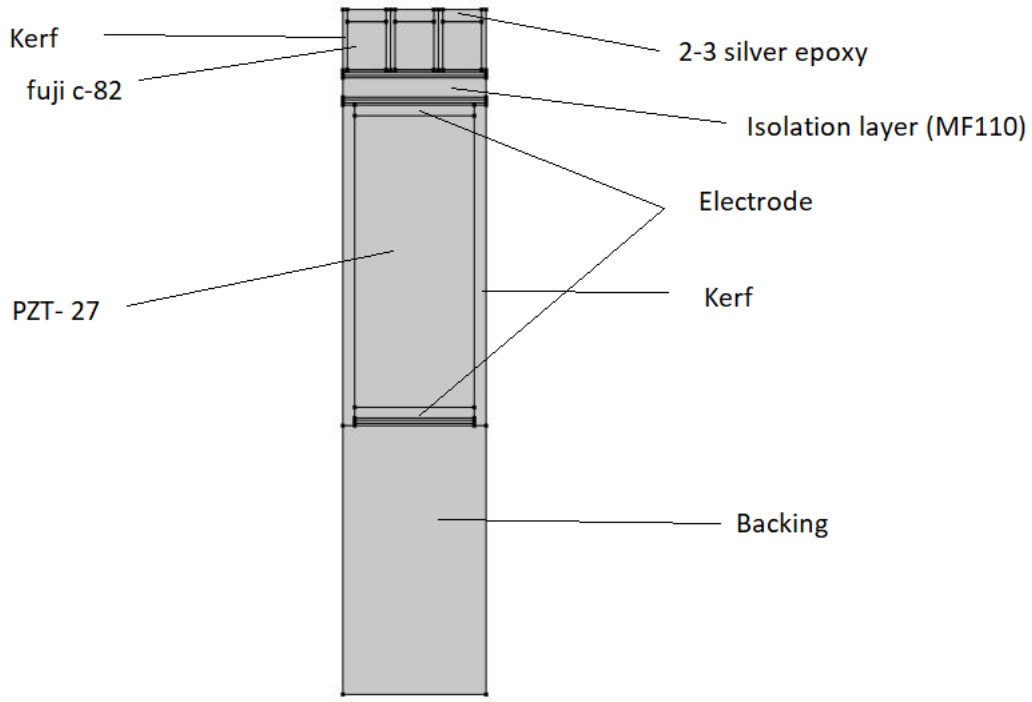

Figure 3.25: FEM model used in COMSOL for dual frequency transducer array.

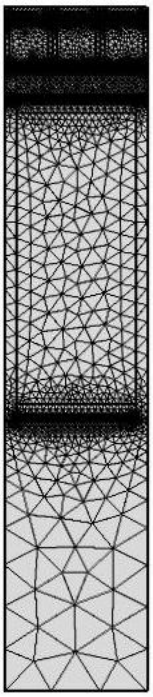

Figure 3.26: Optimization of mesh simulation

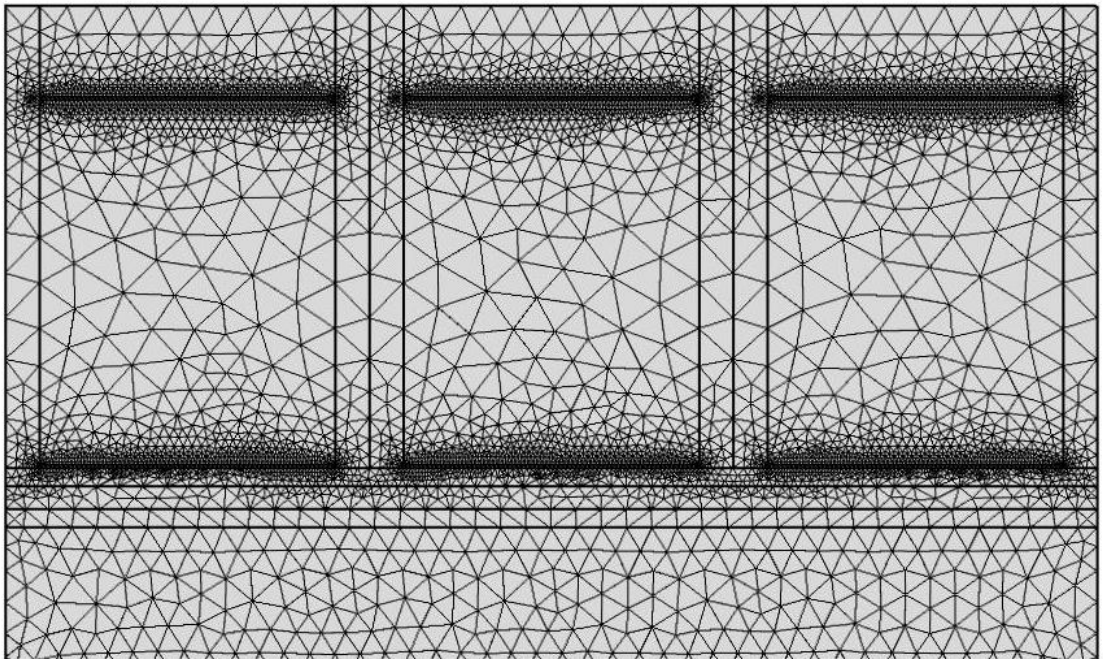

Figure 3.27: Optimization of mesh simulation

The FEM for array ultrasonic transduction was constructed using COMSOL Multiphysics 5.2a acoustic-piezoelectric interaction module in the frequency domain. This model is investigated in two dimensional spaces (2D). The results of the measurements were verified by the COMSOL model under the Acoustic-Piezoelectric Interaction Physics Package with the following boundary condition: periodic boundary condition was applied on the kerf and rest of the structure is free, the electrical potential and the ground are applied to the upper and lower sides of the piezoelectric material for 20 MHz transducer and electrical potential and ground was applied on lower and upper side of piezoelectric material for 4 MHz transducer . In order to visualize the characteristics of the vibration mode, we can check the animation of deformed form at a fixed frequency. The vibration was obtained by plotting the displacement field.

The electrical impedance of array transducer is given by:

$$Z = \frac{V}{I} \qquad 3.5$$

Where V is the potential difference voltage across the two piezoelectric material faces and I is the current flowing inside.

The electric current following in the element is given by:

$$I = b * \int_0^d j dx \qquad 3.6$$

Where ***j*** is the current density component along y axis, d is the piezoelectric material width, b is the length of each element. In this case, b = 3 mm.

3.6 Field II

Field II was developed by Jorgen Jensen at the technical university of Denmark. Basically it is used to simulate the ultrasound imaging based on spatial impulse response. It consists of C programming and number of MATLAB m-function that is used to call the Field II program.

Field II consists of m-function. These m-functions are used to define and manipulate transducers and to perform calculations.

Following are the sequence followed by simulation:

- Make a field II model of the transducer array
- Simulate the beam profile at steering angle (0^0 ,10^0)

The transducer array for phased imaging was defined and the array specifications for both 20 Mhz and 4 Mhz transducer are summarized in Table 9 and 10 respectively.

Table 9: Transducer array specification for 20 MHz

Parameters Name	**Values**
Center Frequency	20 MHz
Sample frequency	100 MHz
Number of elements	70
Width	60 um
Kerf	15 um
Pitch	80 um
Height	3 mm

Table 10: Transducer array specification for 4 MHz

Parameters Name	**Values**
Center Frequency	4 MHz
Sample frequency	100 MHz
Number of elements	22
Width	200 um
Kerf	40 um
Pitch	240 um
Height	3 mm

4 CHAPTER RESULTS

4.1 Single Element Transducer

4.1.1 Impedance measurement of single element transducer

Fig. 4.1 shows the electrical impedance in air of the single element low frequency transducer experimentally using an impedance analyzer and by simulation using the 1-D mason model. For the PZT, the simulated impedance magnitude was 93 Ohms at a series resonance frequency of 3.9 MHz while the experimental impedance curve showed a series resonance of 66 Ohms at 3.9 MHz. The curves are very similar, but some difference in damping.

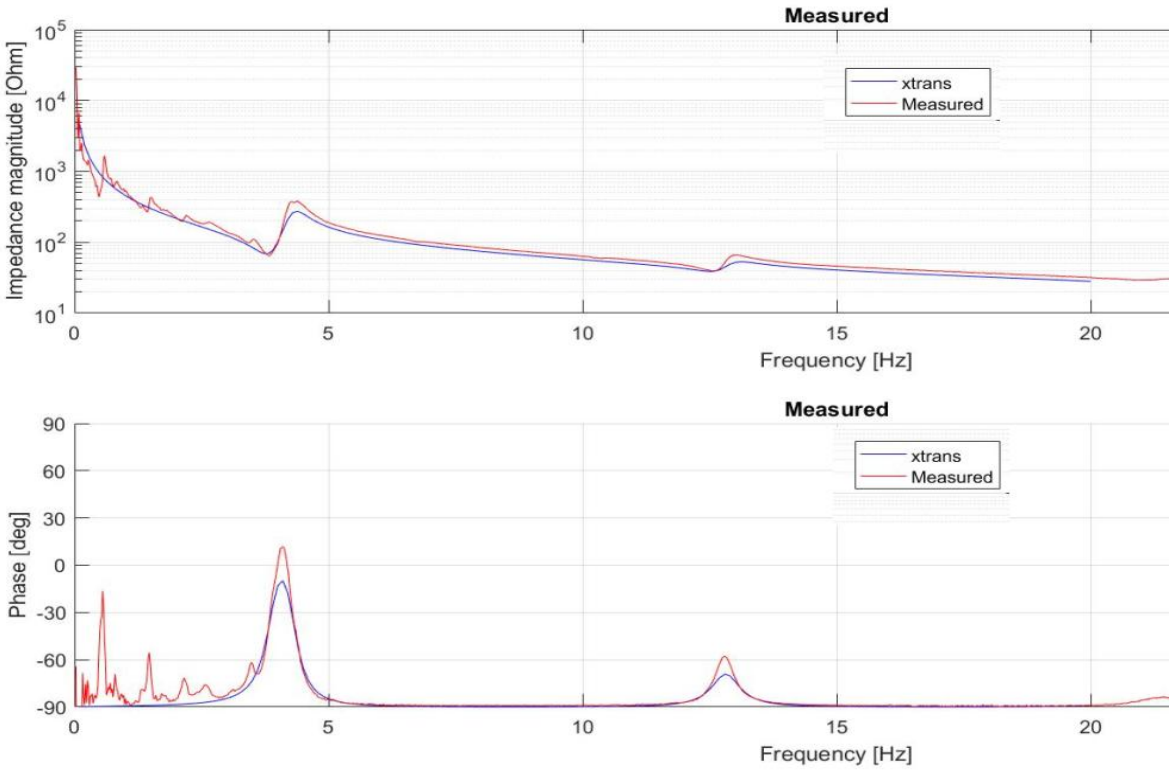

Figure 4.1: Electrical impedance of single element transducer.

4.2 Low Frequency Transducer Array

4.2.1 Impedance measurement of an element in low frequency transducer array

Fig. 4.2 shows the electrical impedance in air of an element of low frequency transducer array experimentally using a network analyzer and by simulation using the FEM Comsol model. The curves are very similar, but some difference in damping. The impedances are too high for good measurements with the network analyzer. And I can try to smooth them.

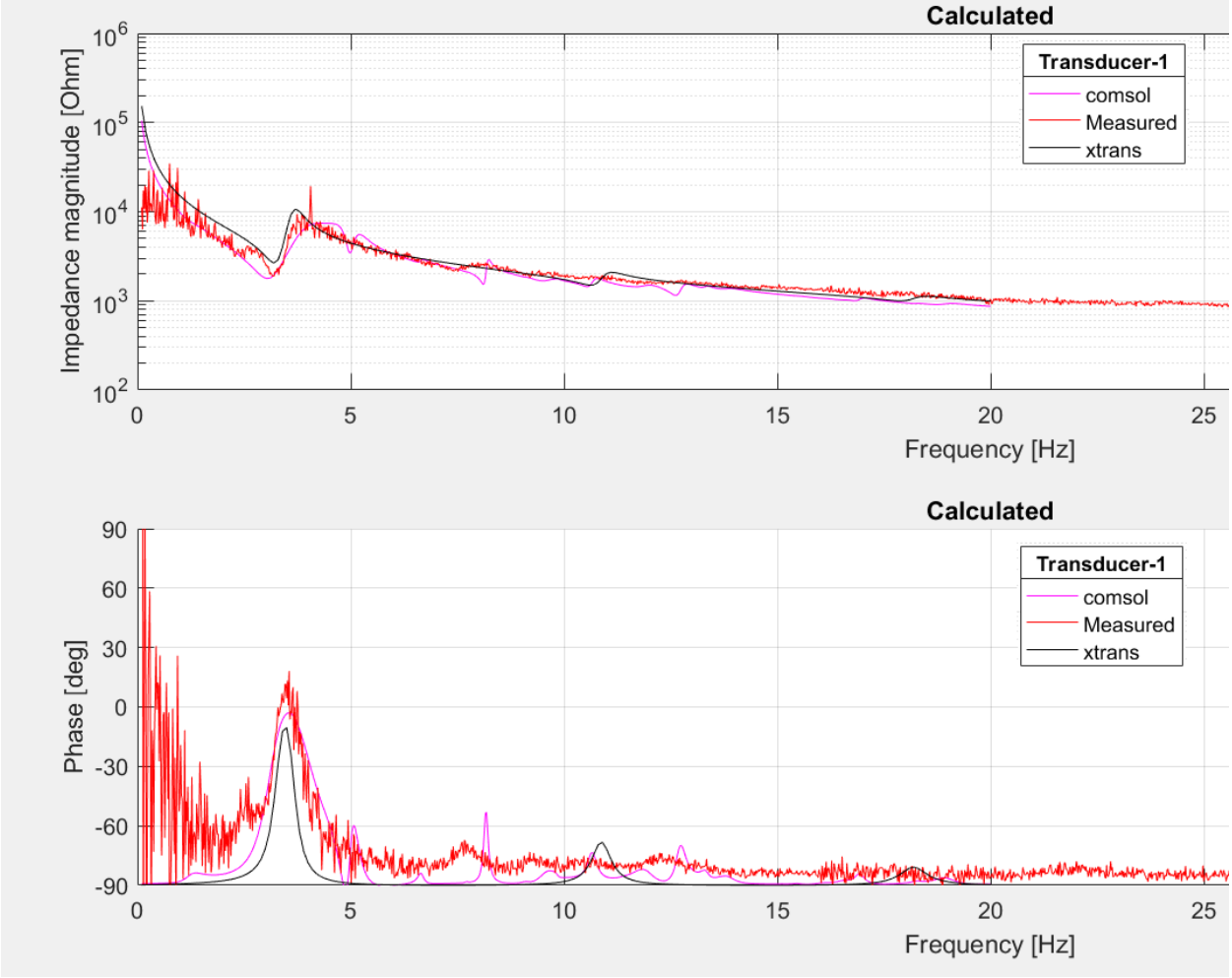

Figure 4.2: Electrical impedance of low frequency transducer array.

4.2.2 Variation in Electrical Impedances

Figure 4.3 showed the experiment confirmed that as the element width decreases, the resonant peak shifts down from 7.911 MHz to 7.706 MHz, Element width variance approximately from 190µm to 205µm was found to create a downward shift of the width-extensional mode. In addition, no measurable effect on resonance at thickness mode was observed shifts. Figure 4.4 shows the real shape of the kerf and element width after dicing.

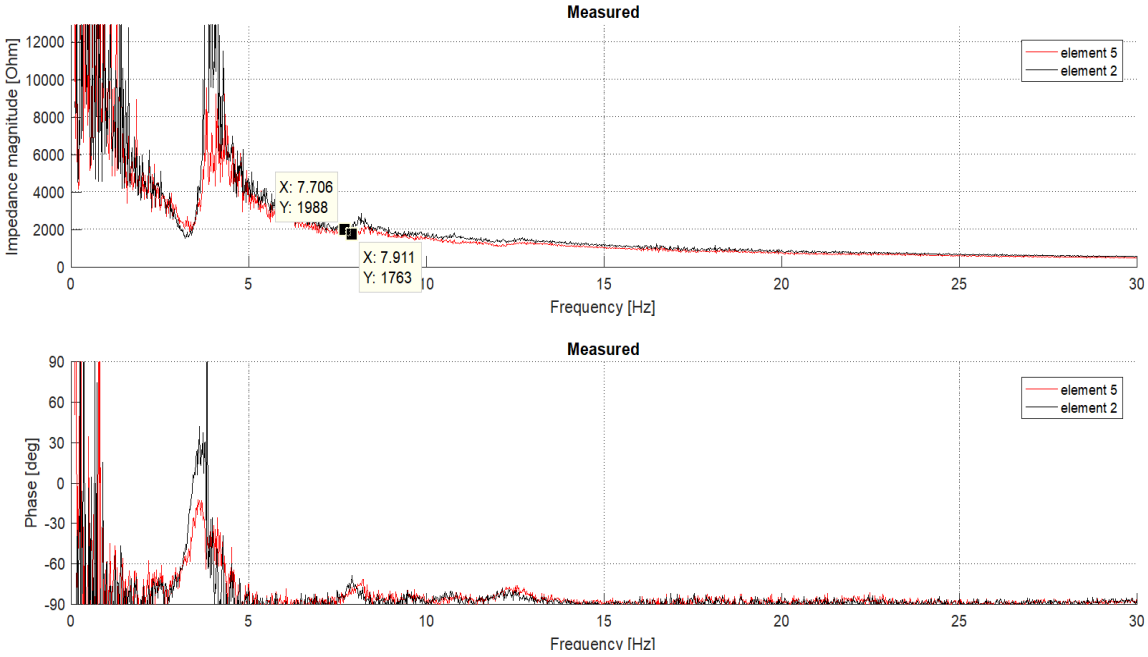

Figure 4.3: Electrical impedances with different element widths

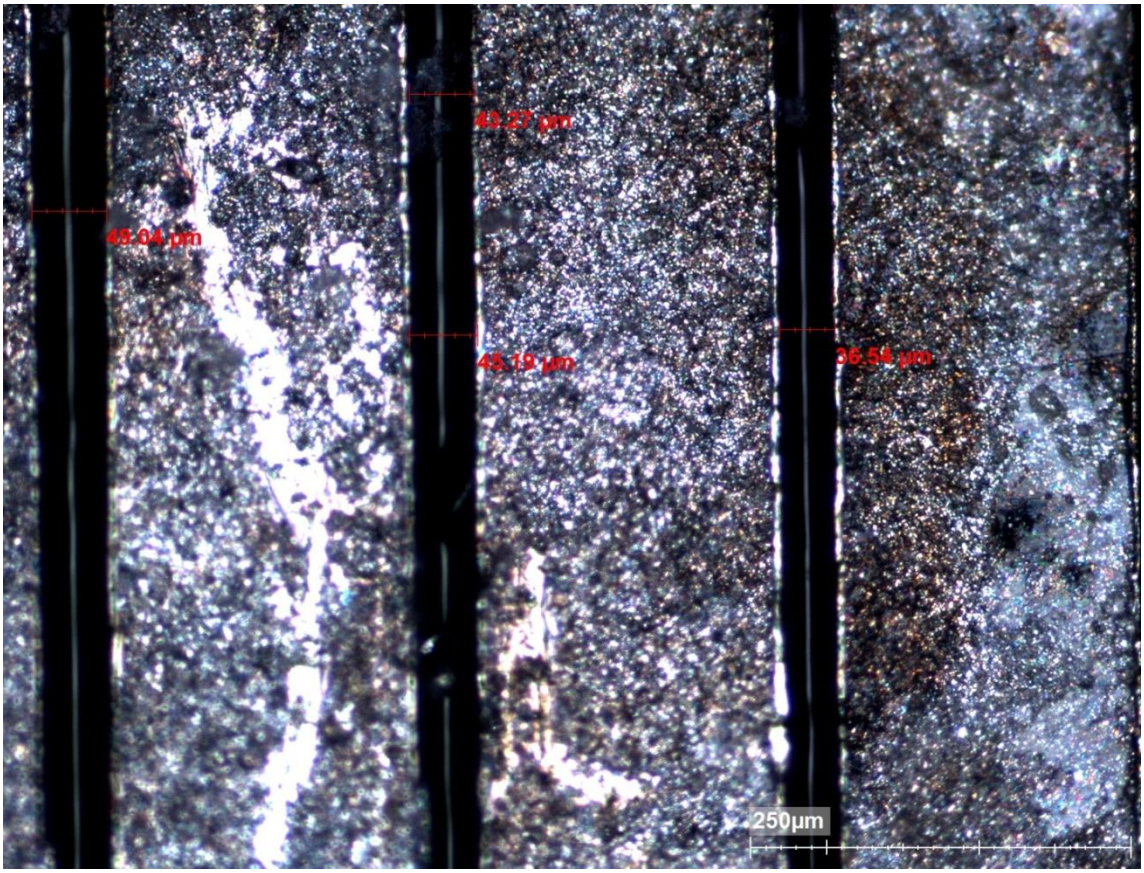

Figure 4.4: Figure 4.5: Microscopic image of the array after dicing, showing the actual shape of kerf and element width. The kerfs are seen as grey lines, while the elements are lighter black/white patterns

4.2.3 Field II program and Beam profile simulation

By using the parameters listed in Table 10, array model was made by using field II program and the beam profile was simulated at the steering angle 0^0, 10^0 respectively as shown in figure 4.5 and 4.6.

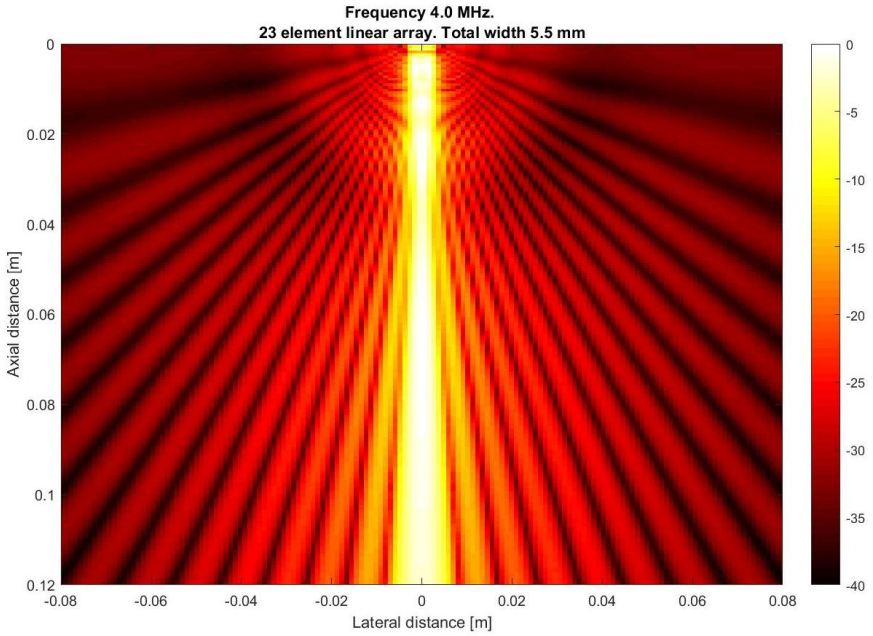

Figure 4.6: Beam profile for 23 bit element array steered at $\theta=0^0$.

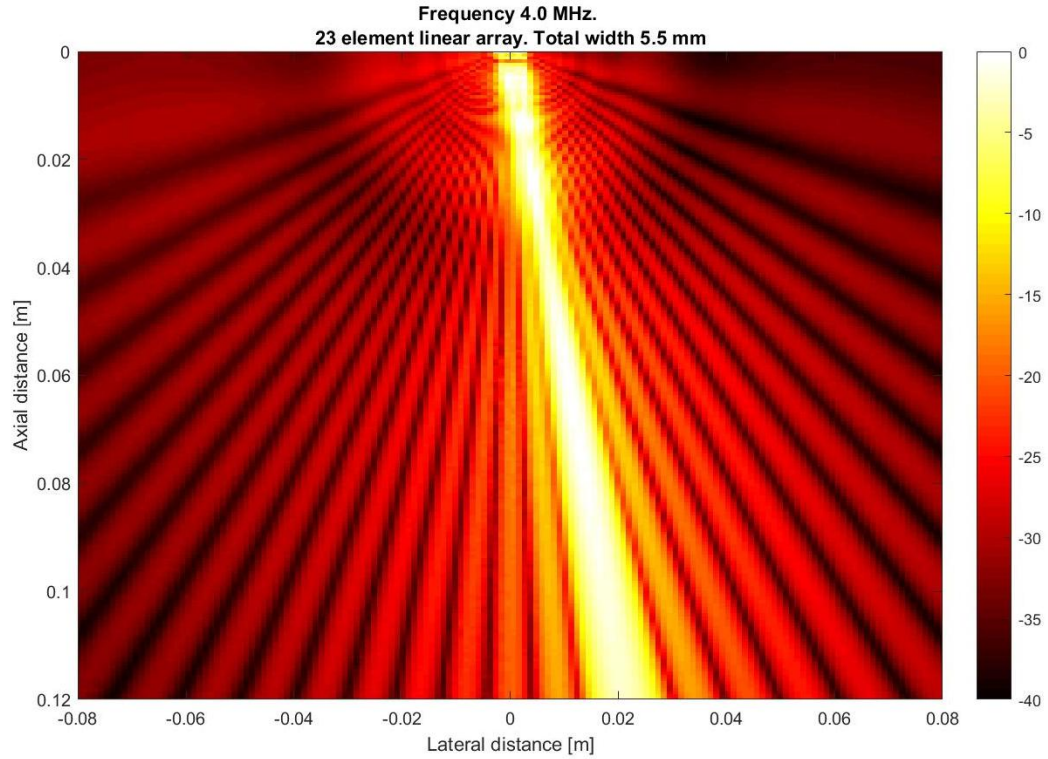

Figure 4.7: Beam profile for 23 bit element array steered at $\theta=10^0$

4.3 High Frequency Transducer Array

4.3.1 Pulse-echo simulation

Simulated result of high frequency transducer using KLM model [23] is shown in figure 4.7. Simulated data is given in table 11.

Table 11: Simulated data from KLM model

Level dB	Center Frequency MHz	Band Width MHz	Band Width % CF
-6	20.390	17.839	87.49
-20	21.521	27.474	127.66
-40	22.163	38.171	172.23

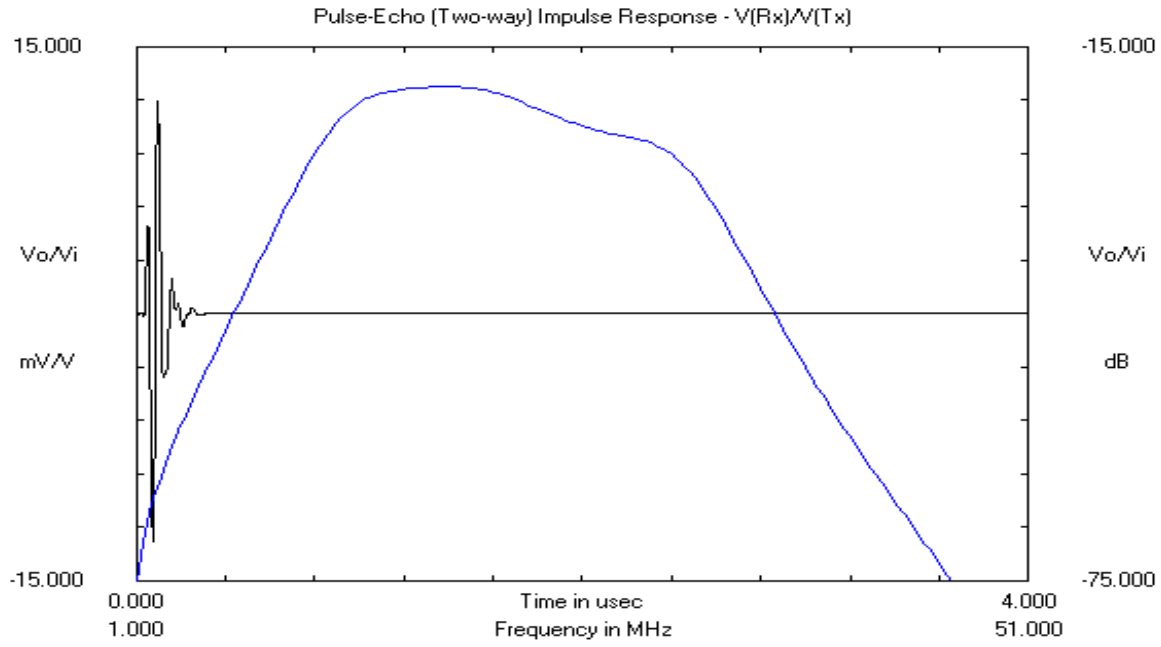

Figure 4.8: KLM simulation of pulse echo test of 20 MHz transducer array.

4.3.2 Impedance measurement of low frequency transducer array

Fig. 4.8 Shows the electrical impedance in air of an element of high frequency transducer array experimentally using an impedance analyzer and by simulation using the 1-D mason model. The curves are similar, but the measured peaks are more damped.

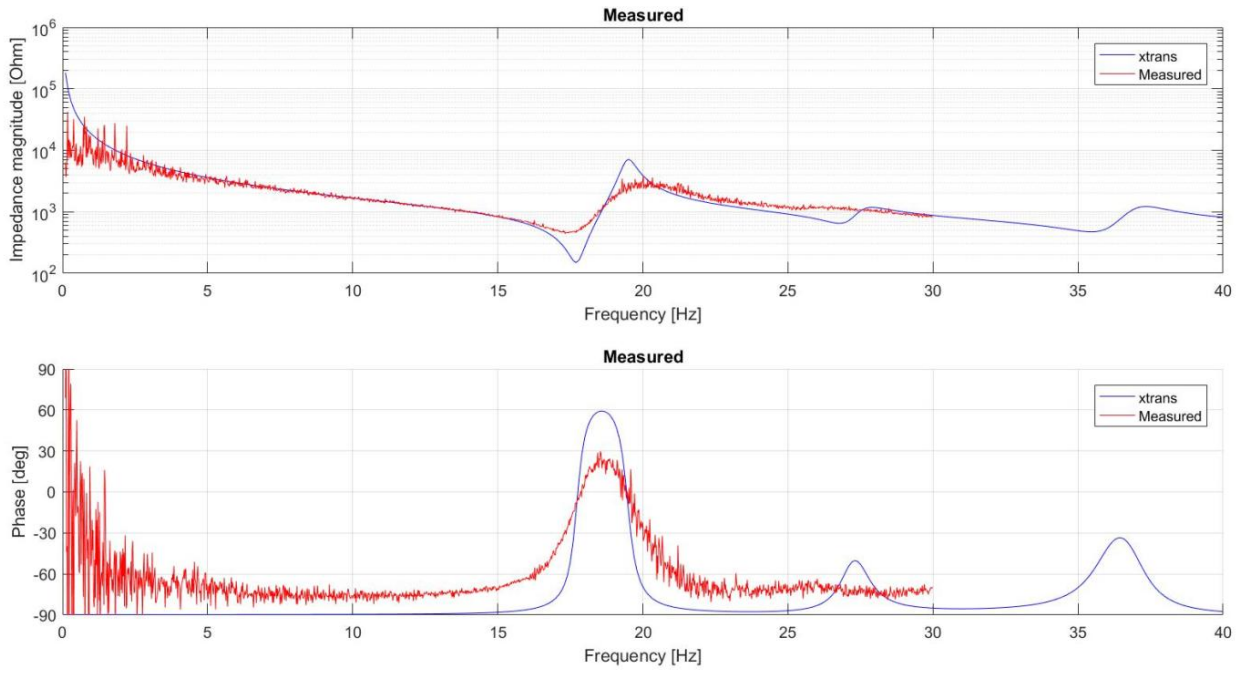

Figure 4.9: Electrical impedance in air of high frequency transducer array

4.3.3 Variation in kerf

Figure 4.9 Microscopic image of the array after dicing, showing the actual shape of kerf and element width. The kerfs are seen as grey lines, while the elements are lighter black/white patterns. Kerf = pitch – element width.

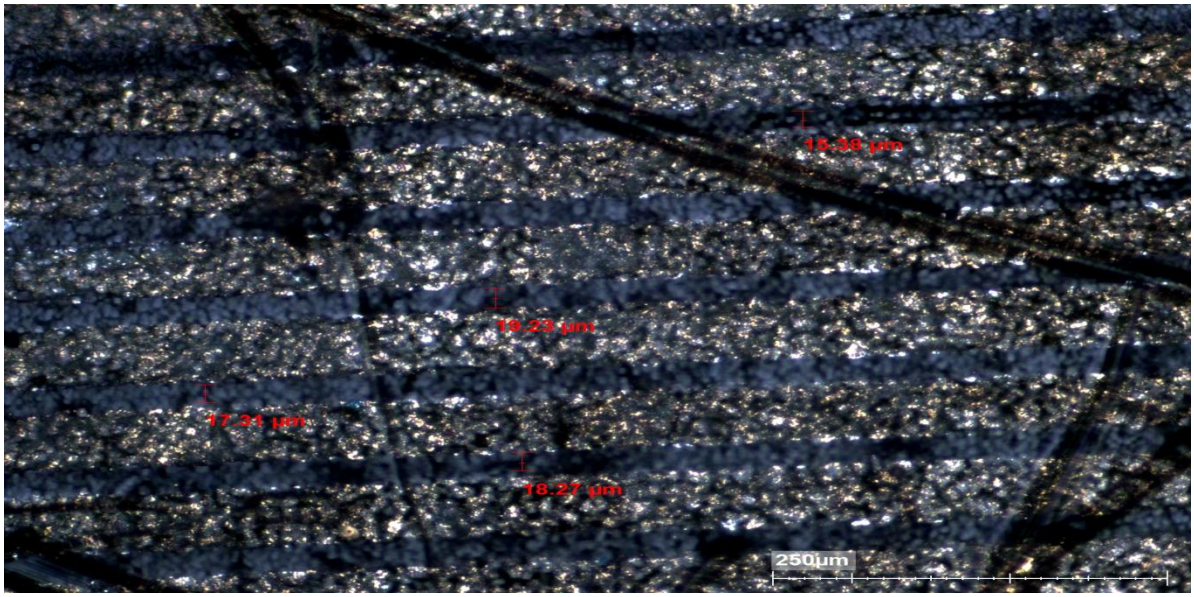

Figure 4.10: Microscopic image of the array after dicing, showing the actual shape of kerf and element width. The kerfs are seen as grey lines, while the elements are lighter black/white patterns

4.3.4 Field II program and Beam profile simulation

By using the parameters listed in Table 9, array model was made by using field II program and the beam profile was simulated at the steering angle 0^0, 10^0 respectively as shown in figure 4.10 and 4.12. Grating lobes were expected, as fabrication limited the minimum pitch, and the design is a test structure to investigate the structures. It will not be suited for imaging.

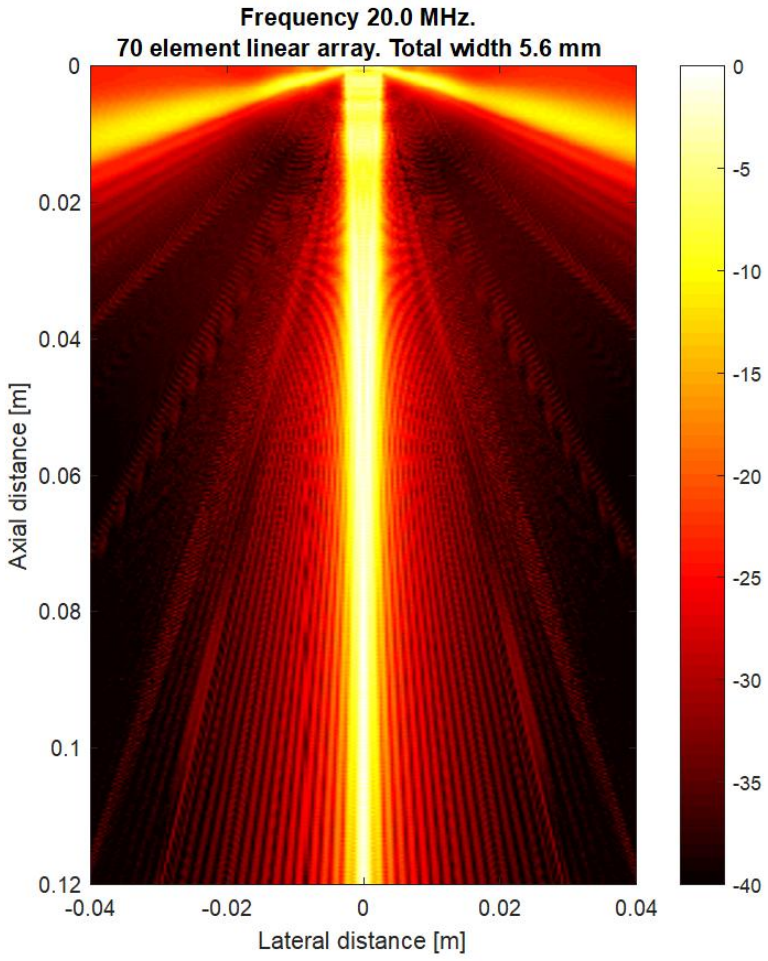

Figure 4.11: Beam profile for 70 bit element array steered at $\theta=0^0$.

Figure 4.11 and Figure 4.13 shows the theoretical model which have no side lobes and the data are presented in table 12.

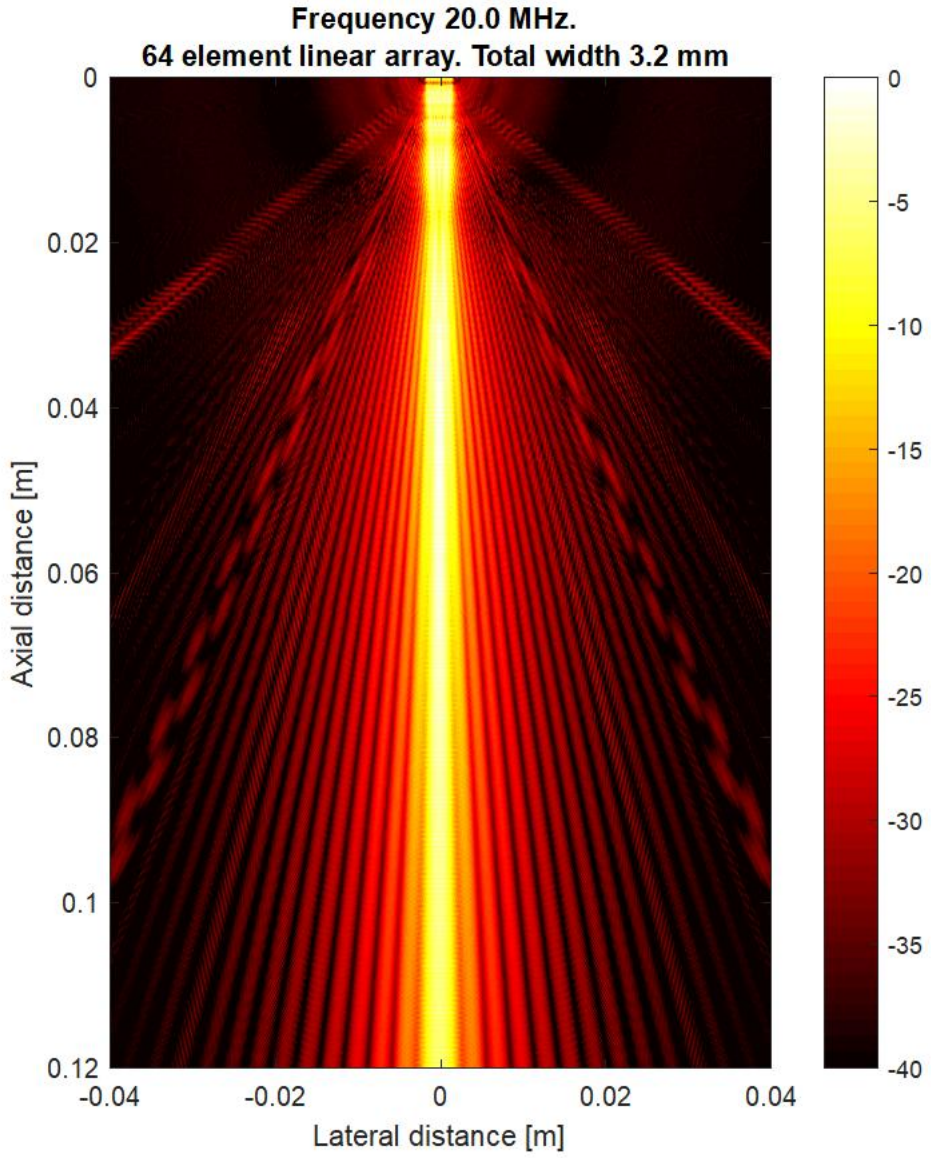

Figure 4.12: Beam profile for 64 bit element array steered at $\theta=0^0$.

Table 12: Theoretical Transducer array specification for 20 MHz transducer array

Parameters Name	**Values**
Center Frequency	20 MHz
Sample frequency	100 MHz
Number of elements	64
Width	40 um
Kerf	15 um
Pitch	50 um
Height	3 mm

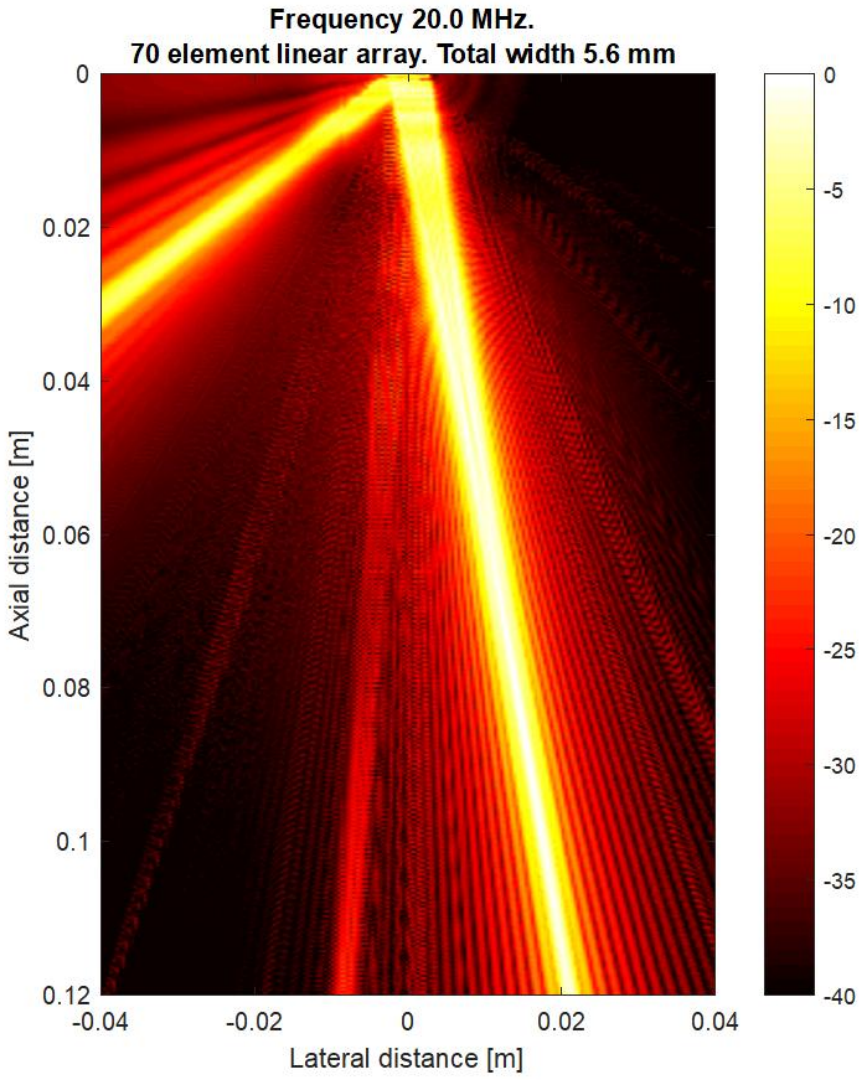

Figure 4.13: Beam profile for 70 bit element array steered at $\theta=10^0$.

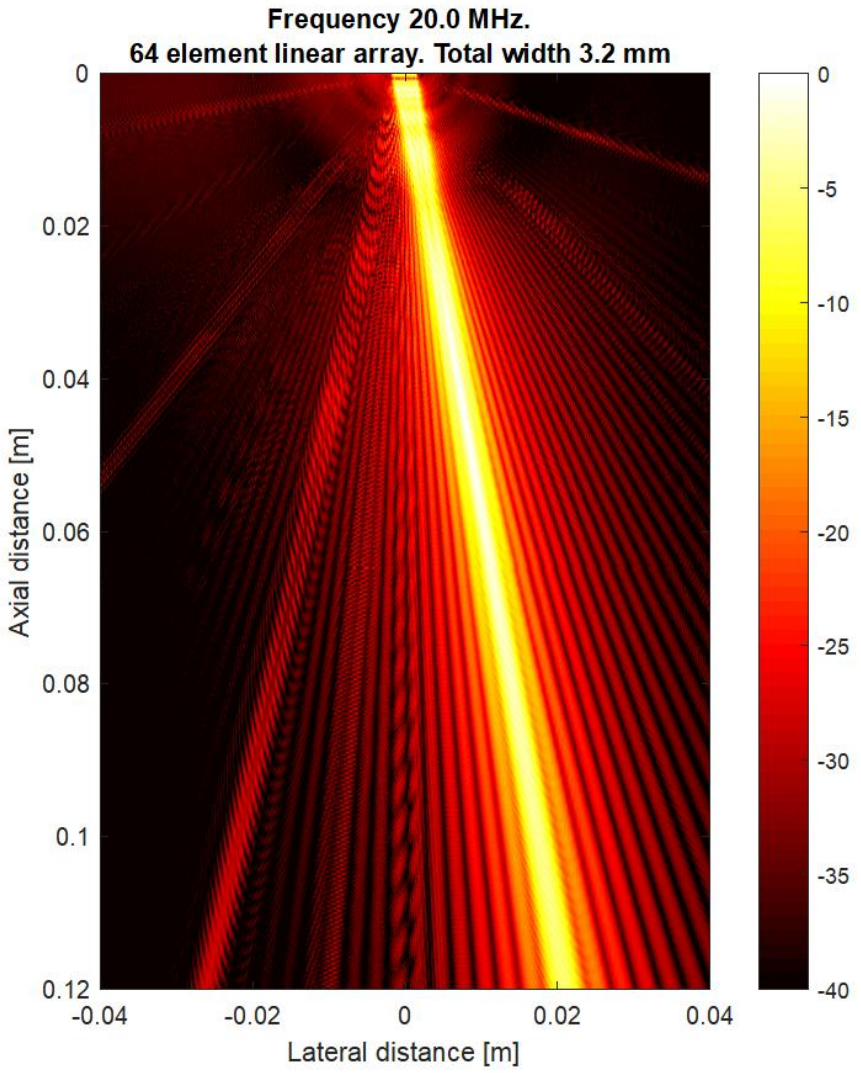

Figure 4.14: Beam profile for 64 bit element array steered at $\theta=10^0$.

4.4 Flexible circuit design

Flexible circuit was designed on Altium Designer 17 ™ with two layers as shown in figure 4.14. It used for electrical characterization of transducer array. Need of the flex circuit is to connect the elements separately.

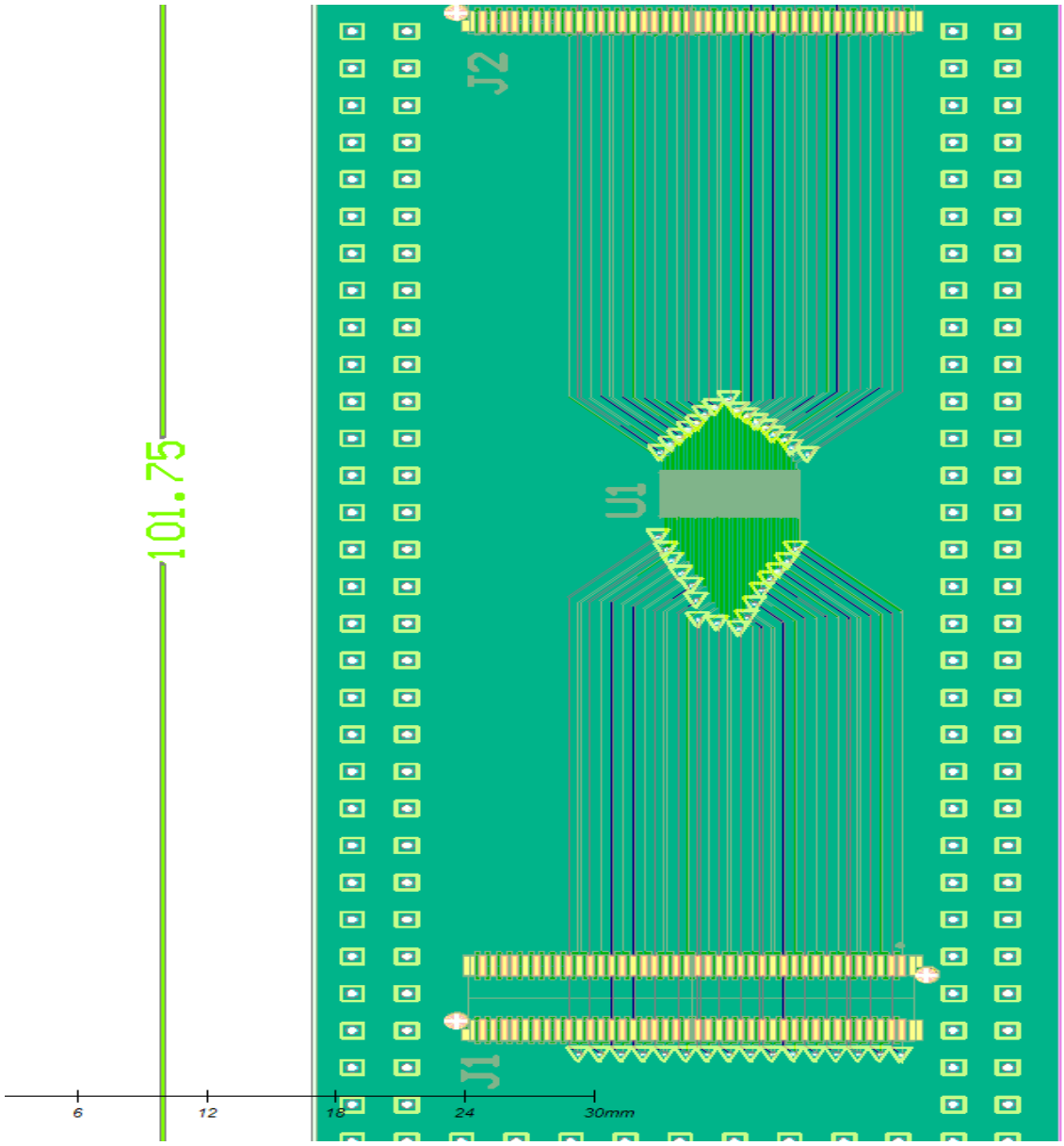

Figure 4.15: Flexible circuit.

4.5 Dual Frequency Transducer Array

4.5.1 Electrical impedance measurement

Electrical impedance measurement of dual frequency transducer is shown in figure 4.15. In the figure below impedance measurement was taken place when low frequency stack was active and high frequency stack was passive. The mason model and measured curve are similar but the result from comsol is not matched and is more damped.

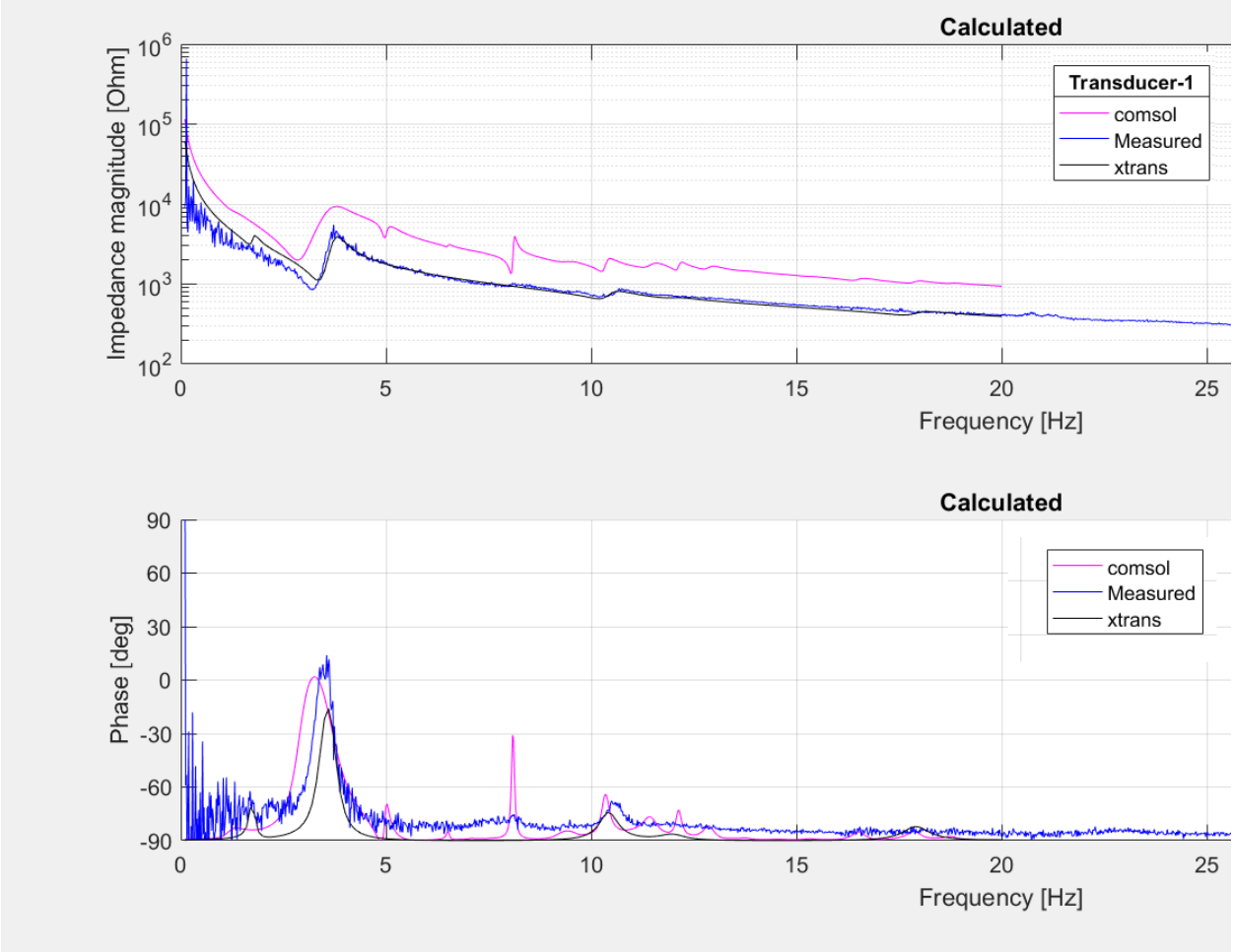

Figure 4.16: shows the electrical impedance in air of dual frequency transducer array when LF was active and HF was passive

Figure 4.16 shows impedance measurement of dual frequency transducer when high frequency transducer was active and low frequency transducer was passive. In this case the high frequency transducer array was working as we can see from the figure 4.16 that we are getting the thickness mode around 20 MHz. The measured and calculated curves looks similar but only measured curves are more damped.

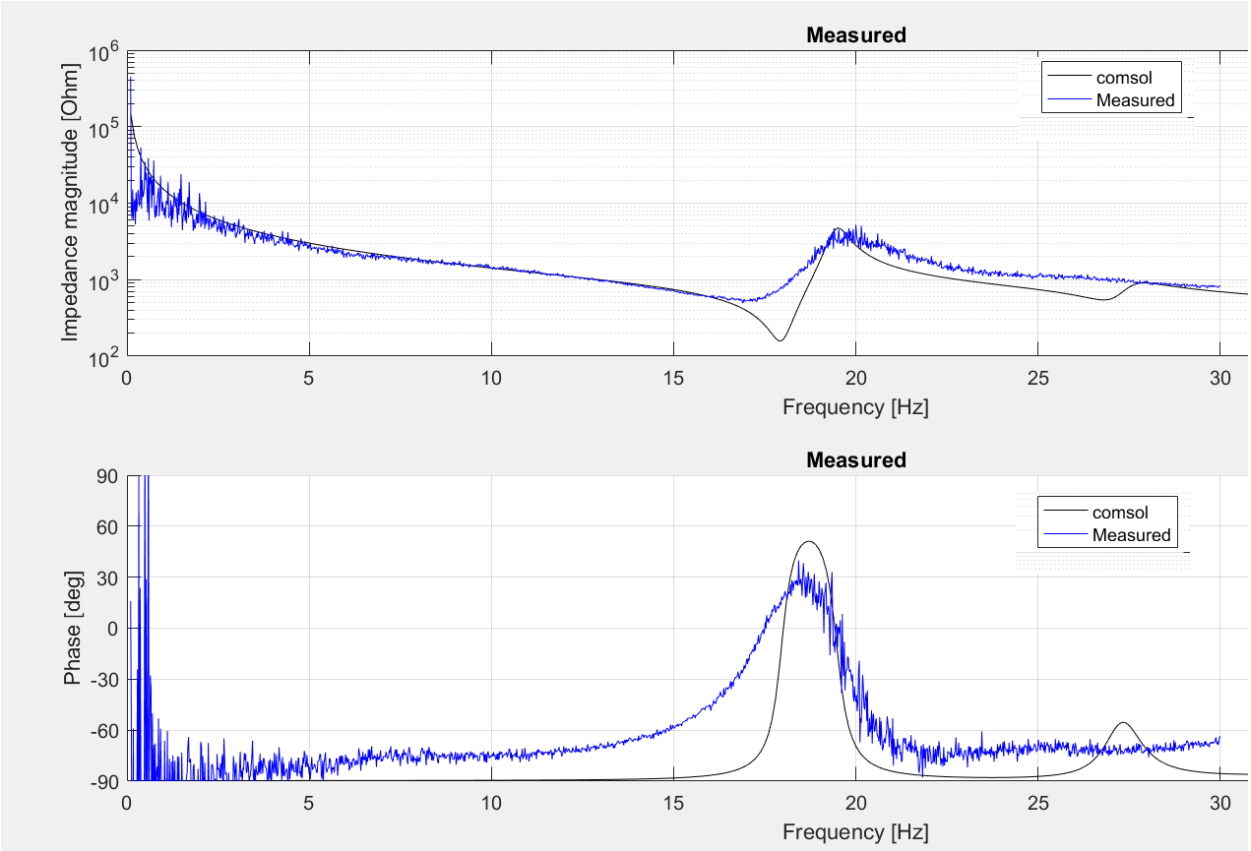

Figure 4.17: shows the electrical impedance in air of dual frequency transducer array when LF was passive and HF was active

5 CHAPTER DISCUSSION

In this chapter, the agreement between measurements and simulation results is considered to comment the method and model are valuable or unacceptable. The causes of errors that can be appeared are also discussed.

5.1 Single Element Transducer

Our results show that the experimental measurement agrees fairly well with 1-D model simulation models. As we can see from figure 4.1 the anti resonance peak is near about 4 MHz which is the thickness mode peak. For the thickness mode, the vibration is oriented along the direction of polarization. The resonant frequency depends on the thickness of the device; therefore, a thin plate implies a high frequency drive. For the radial mode, the direction of vibration is oriented orthogonal to the direction of polarization. The diameter in the direction of propagation of this mode is much greater than its thickness. Since the resonant frequency depends on the diameter, hence a large length implies a low resonant frequency drive. As we can see the lateral mode was not captured by 1-D model because it one- dimensional model and It only calculate the thickness mode.

5.2 Low Frequency Transducer Array

5.2.1 Impedance measurement of an element in low frequency transducer array

Our overall results suggest that the close agreement between simulation and measurements strongly confirms the validity of our simulation process. As we can see in figure 4.2 the experimental result shows a lot of noise. The high impedance is difficult to measure by the network analyzer and that could be the reason of noisy result.

5.2.2 Variation in Electrical Impedances

Our finding confirms that variation in element width may origin from vibration of blade operating at different revolution speeds. This variation causes downshift at frequency around 7.7 MHz because width-extensional resonant mode is present at that frequency shown in figure 4.3. This phenomenon makes perfect sense because element width is inversely proportional to

resonance frequency at this mode. Element width has no large effect on thickness vibration mode.

5.2.3 Beam profile simulation

The beam profile simulation shows that there is no grating lobes present in the figure when it steered at 0^0 and 10^0. Grating lobes are the maxima of the main beam, as predicted by the pattern multiplication theorem. When the array spacing is less than or equal to λ/2, only the main lobe exists in the visible space, with no other grating lobes. Grating lobes appear when the array spacing is greater than λ/2. The generation of unwanted grating lobes or side lobes, two closely related phenomena caused by sound energy that spreads out from the transducer at angles other than the primary path. For large spacing, grating lobes can appear in the visible space even at a zero scan angle. These unwanted ray paths can reflect off surfaces in the test piece and cause spurious indications on an image. The amplitude of grating lobes is significantly affected by pitch size, the number of elements, frequency, and bandwidth.

5.3 High Frequency Transducer Array

Data for Pulse-echo simulation of high frequency transducer using KLM is given table 11. As we can see that we got 87 % bandwidth at 20.23 MHz center frequency which is more than our minimum requirement i.e. 80 %. The imaging frequency shall be optimized for image resolution, i.e. high bandwidth and short pulses this was the reason for designing such high bandwidth transducer. But unfortunately we were unable to measure the pulse-echo because the pulse echo setup was not optimized for high frequency transducer.

The measured impedance and I D model impedance is close but the simulated curve was not captured by the measured value. Level outside resonances are well reproduced and measured resonance peaks is not as sharp as predicted by theory and it is also over damped, the data we got for mechanical quality factor and coupling factor is not 100 percent accurate and that could be the reason for variation between measured and theoretical value. The high impedance was difficult to measure by the network analyzer this could be the cause for noisy signal. 1-D model works only in thickness mode so, there is no lateral mode are present in the simulated signal. Quite strong mismatch between measured and calculated because the fabricated structures were not as described that could be the reason. While measuring the impedance of high frequency

transducer array with the help of medical needle the tip of needle was not small enough to touch one element at a time even working under the microscope and when you puncture the parylene several time some part of the parylene came off from top the transducer which makes the thickness of transducer uneven. That also could be the reason of mismatch.

5.3.1 Beam profile simulation

In figure 4.10 we can see that there is no grating lobe present because the beam was steered at an angle 0^0. But clearly it started to appear as we can see on the top. When we steered the beam at an angle 10^0. We clearly got the grating lobes shown in figure 4.12. Grating lobe is present because result of fabrication i.e. we could not reach sufficiently fine pitch and we were aware of this but made it to test the procedure. The model without grating lobe is presented in figure 4.11 and figure 4.13. Grating lobes will occur whenever the size of individual elements in an array is equal to or greater than the wavelength, and there will be no grating lobes when element size is smaller than half a wavelength. (For element sizes between one-half and one wavelength, the generation of grating lobes will depend on the steering angle.). Grating lobes appear when the array spacing is greater than $\lambda/2$. In this thesis the pitch of the high frequency transducer array is 80um which is greater than the wavelength. Array was constructed with grating lobes because of the fabrication limitations. These are test structures to investigate the and learn, and grating lobes were accepted for this purpose, as there was no option to make a n array with sufficiently fine pitch.

5.4 Dual Frequency Transducer Array

Figure 4.15 shows the impedance measurement of dual frequency transducer when high frequency stack works as a passive layer and low frequency stack work as an active layer. Measured signal and simulated signal from 1-D model were fitted well but signal from comsol model is not fitted well. Data for high frequency transducer not 100 % accurate and that could be

the reason for this. The high impedance was difficult to measure by the network analyzer this could be the cause for noisy signal. Unfortunately we were unable to test the dual frequency transducer array at same time reason for this is explained in challenges.

Figure 4.16 shows the impedance measurement of dual frequency transducer when high frequency stack works as an active layer and low frequency stack work as a passive layer. Level outside resonances are well reproduced and measured resonance peaks is not as sharp as predicted by theory and it is also over damped, the data we got for mechanical quality factor and coupling factor is not 100 percent accurate and that could be the reason for variation between measured and theoretical value. The high impedance was difficult to measure by the network analyzer this could be the cause for noisy signal.

5.5 Challenges

First challenge was to fabricate high frequency transducer array within two and half month. Second challenge was to get the flex circuit which I designed for the transducer array shown in figure 4.14. The only vendor who is making the flex with 80 um pitch is MicroConnex Corporation 34935 SE Douglas St #110, Snoqualmie, WA 98065, USA [29]. Prices for the flex in this corporation was quite expensive so, couldn't able buy it. Real challenge started after this i.e. how test the transducer array without proper electrical connection. One side of the transducer was covered by parylene which is purely non conductive. Since, the one side covered by parylene (which is also the second matching layer for the transducer) it was hard to get the ground for impedance measurement. We started by connecting the back side with copper and puncturing the parylene layer with medical needle which was connected with network analyzer. Puncturing of the parylene was performed under the microscope, we were finally able to get some impedance measurement but the first consequences of this, we were unable to perform the impedance measurement for all the elements. Second, consequences were the tip of needle was not small enough to touch one element at a time even working under the microscope and the third consequence was, when you puncture the parylene several time some part of the parylene came off from top the transducer which makes the thickness of transducer uneven. This is why

we were unable measure the impedance of dual frequency transducer with both the stack as an active layer.

After all the challenges we were able to get some impedance measurement. These transducers were not made for some particular application. The purpose was to fabricate and test the dual frequency transducer.

6 CHAPTER CONCLUSION

6.1 Thesis contribution

In this thesis, the dual frequency array transducer was fabricated and characterized. The array was fabricated as an acoustic stack with two piezoelectric layers, one 'pumping' low frequency at around 4MHz, and one 'imaging' high frequency, around 20MHz. The measured and simulated values for low frequency transducer array are fabricated and characterized. We also compared the two elements. The experiment confirmed that as the element width decreases, the resonant peak shifts down from 7.911 MHz to 7.706 MHz, Element width variance approximately from 190μm to 205μm was found to create a downward shift of the width-extensional mode. The beam profile measurement without any grating lobes is found for the low frequency transducer array.

The fabrication and characterization of high frequency transducer array was done. The impedance measurement of high frequency transducer was characterized and the high impedance was difficult to measure by the network analyzer this could be the cause for noisy signal. The pulse echo measurement in KLM model using piezocad has been done. We were unable to measure it experimentally. The beam profile measurement steered at 0^0 and 10^0 has been done but the grating lobe is present because the pitch was greater than wavelength and was aware of this, but made it to test procedure. The transducer without any grating lobe is also present in this thesis.

The characterization of dual frequency transducer has been done with LF transducer as an active layer and high frequency transducer as a passive layer and vice versa. The flex circuit was designed using altium designer. The high impedance was difficult to measure by the network analyzer this could be the cause for noisy signal. One important contribution is the testing and implementing fabrication procedures, and also I found identified difficulties in fabrication and deviations from theory. This is something we learn from, and is an important contribution to our group

6.2 Future works

Based on the results presented in this thesis, several interesting directions for future work are described as follows:

- Fabricate a dual frequency array transducer with a proper flex, test each element individually and together compare it with FEM model.
- Fabricate low frequency stack with matching layer and compare with FEM model.
- Fabricate dual frequency transducer array with lens.

REFERENCES

[1] Akasheh, F.; Myers, T.; Fraser, J.D.; Bose, S.; Bandyopadhyay, A. Development of piezoelectric micromachined ultrasonic transducers. Sens. Actuators A Phys. 2004, 111, 275–287.

[2] Wang, Z.; Zhu, W.; Miao, J.; Zhu, H.; Chao, C.; Tan, O.K. Micromachined thick film piezoelectric ultrasonic transducer array. Sens. Actuators A Phys. 2006, 130, 485–490.

[3] Akasheh, F.; Fraser, J.D.; Bose, S.; Bandyopadhyay, A. Piezoelectric micro machined ultrasonic transducers: Modeling the influence of structural parameters on device performance. IEEE Trans. Ultrason. Ferroelectr. Freq. Control 2005, 52, 455–468.

[4] Lukacs, M.; Sayer, M.; Foster, S. Single element high frequency (<50 MHz) PZT sol gel composite ultrasound transducers. IEEE Trans. Ultrason. Ferroelectr. Freq. Control 2000, 47, 148–159.

[5] Lawrence E. Kinsler, Austin R. Frey, Alan B. Coppens, and James V. Sanders, Fundamentals of Acoustics. New York: John Wiley & Sons, 1982

[6] Desilets CS, Fraser JD, and Kino GS, "The design of efficient broad-band piezoelectric transducers," IEEE Trans Sonics Ultrason, p. 25:115–25, 1978.

[7] Goldberg, RL., and Smith, SW, The biomedical engineering handbook. CRC Press, 1994.

[8] Richard L. Goldberg, Michael J. Jurgens, David M. Mills, Craig S. Henriquez, David Vaughan, and Stephen W. Smith, "Modeling of Piezoelectric Multilayer Ceramics Using Finite Element Analysis," IEEE Trans. Ultrason. Ferroelectr. Freq. CONTROL, vol. 44, Nov. 1997.

[9] L. Spicci, and M. Cati, "Design and Optimization of a High Performance Ultrasound Imaging Probe Through FEM and KLM Models", in COMSOL Conference, 2011.

[10] T. A. Ritter, T. R. Shrout, R. Tutwiler, and K. K. Shung, "A 30-MHz piezo-composite ultrasound array for medical imaging applications," IEEE Trans. Ultrason. Ferroelectr. Freq. Control, vol. 49, no. 2, pp. 217–230, Feb. 2002.

[11] K. K. Shung and M. Zippuro, "Ultrasonic transducers and arrays," IEEE Eng. Med. Biol.Mag., vol. 15, no. 6, pp. 20–30, Nov. 1996.

[12] K. Kirk Shung, Diagnostic Ultrasound : imaging and blood flow measurements.

[13] J. Krautkramer and H. Krautkramer, Ultrasonic Testing of Materials, Springer-Verlag 1983.

[14] A. Carovac, F. Smajlovic, and D. Junuzovic, "Application of Ultrasound in Medicine," Acta Inform. Medica, vol. 19, no. 3, pp. 168–171, Sep. 2011.

[15] K. K. Shung and M. Zippuro, "Ultrasonic transducers and arrays," *IEEE Eng. Med. Biol.*

[16] *Mag.*, vol. 15, no. 6, pp. 20–30, Nov. 1996.

[17] T. A. Ritter, T. R. Shrout, R. Tutwiler, and K. K. Shung, "A 30- MHz piezo-composite ultrasound array for medical imaging applications," IEEE Trans. Ultrason. Ferroelectr. Freq. Control, vol. 49, no. 2, pp. 217–230, 2002.

[18] Jonathan M. Cannata, Member, IEEE, Jay A. Williams, Lequan Zhang, Chang-Hong Hu, and K. Kirk Shung, Fellow, IEEE .A High-Frequency Linear Ultrasonic Array Utilizing an Interdigitally Bonded 2-2 Piezo-Composite .

[19] “High quality components and materials for the electronic industry,” Hejreskovvej 18A DK-3490 Kvistgard, Denmark 2003.
[20] Azuma T, Ogihara M, Kubota J, Sasaki A, Umemura SI, Furuhata H. Dual-frequency ultrasound imaging and therapeutic bilaminar array using frequency selective isolation layer. IEEE Trans Ultrason Ferroelectr Freq Control. 2010; 57(5):1211– 1224. [PubMed: 20442033].
[21] Jianguo Ma, K. Heath Martin, Paul A. Dayton, and Xiaoning Jiang A Preliminary Engineering Design of Intravascular Dual-Frequency Transducers for Contrast-Enhanced Acoustic Angiography and Molecular Imaging.
[22] Ola Finneng Myhre, Johannes Kvam and Bjørn A. J. Angelsen, Dual Frequency Transducer Design for Suppression of Multiple Scattering.
[23] L. P. Tran-Huu-Hue, F. Levassort, N. Felix, D. Damjanovic, W. Wolny, and M. Lethiecq, “Comparison of several method characterise the high frequency behaviour of piezoelectric ceramics for transducer.” ELSEVIER, 2000.
[24] R . Krimholtz, D. A. Leedom, and G. L. Matthei, “New equivalent circuits for elementary piezoelectric transducers,” Electron. Lett., vol. 6, no. 13, pp. 398–399, 1970.
[25] Duy Le-Anh , Tung Manh, Lars Hoff.A Study on Electrical Impedance Variations between Transducer Elements in One-Dimensional Piezoelectric Arrays".
[26] J.Assaad, M. Ravez, C. Bruneel, J.M. Rouvaen, and F. Haine, “Influence of the thickness and attenuation coeficeint of a backing on the response of transducers,” Ultrasonics, vol. 34, pp. 103–106, 1996.
[27] J.E.S.M. Medina, F. Buiochi, and J.C. Adamowski, “Numerical modeling of a circular piezoelectric ultrasonic transducer radiating in water,” ABCM Symposium Series in Mechatronics, vol. 2, pp. 458–464, 2006.
[28] Yasuhide Shindo, Electromagneto-Mechanics of Material Systems and Structures.
[29] Xuecang Geng, Numerical modeling and experimental study of piezocomposite transducers, thesis in materials, Dec 1997.
[30] Yuling Chen, Man Nguyen, and Jesse T. Yen A 7.5 MHz Dual-Layer Transducer Array for 3-D Rectilinear Imaging.